SLAC-PUB-2314
April 1979
(T/E)

HADROPRODUCTION OF MASSIVE LEPTON PAIRS AND QCD*

Edmond L. Berger
Stanford Linear Accelerator Center
Stanford University, Stanford, California 94305

and

High Energy Physics Division**
Argonne National Laboratory, Argonne, Illinois 60439

ABSTRACT

A survey is presented of some current issues of interest in attempts to describe the production of massive lepton pairs in hadronic collisions at high energies. I concentrate on the interpretation of data in terms of the parton model and on predictions derived from quantum-chromodynamics (QCD), their reliability and their confrontation with experiment. Among topics treated are the connection with deep-inelastic lepton scattering, universality of structure functions, and the behavior of cross-sections as a function of transverse momentum.

(Invited talk presented at ORBIS SCIENTIAE 1979, Coral Gables, Florida, January 15-19, 1979.)

---

* Work supported by the Department of Energy under contract number EY-76-C-03-0515.

** Permanent address.

I. Introduction

Massive lepton pair production in hadronic collisions, $h_1 + h_2 \to \ell\bar{\ell}X$, commonly known as the Drell-Yan process,[1-3] measures the ability of interacting hadrons to reconfigure their momentum into the local production of a virtual photon γ^* with four-momentum Q^μ. In the parton model, the production is imagined to occur through the annihilation of a quark from one hadron with an antiquark from the other, in the subprocess $\bar{q}q \to \gamma^* \to \ell\bar{\ell}$; $\ell = \mu, e, \ldots$ The Drell-Yan process can thus be exploited to determine the quark and antiquark structure functions of hadrons in the timelike region, $Q^2 > 0$, and to probe other important aspects of the dynamics of hadronic constituents at short distance.

Not long ago it was an open question whether a high-mass lepton-pair continuum would be observed experimentally with the general qualitative features expected by the Drell-Yan model. Excellent data extending to muon-pair masses of ~15 GeV in pN collisions,[4-8] and to ~11 GeV in π^-N reactions[9-11] have removed most doubts. Although the quantitative consistency of the classical model with data as a function of all kinematic variables (target atomic number A; pair mass M; scaled longitudinal momentum $x_F = Q_L/Q_L^{max}$; pair transverse momentum $\vec{Q}_T$; and decay angles θ^*, ϕ^* in the pair rest-frame) has not been demonstrated in precise detail, the general picture is clear. The focus has changed to other questions.

From the perspective of quantum chromodynamics (QCD), issues of present concern include (a) whether the Drell-Yan prescription is the full answer, and (b) if so, whether constituent structure functions determined for $Q^2 > 0$ via the Drell-Yan mechanism should be, and/or are experimentally observed to be, identical to those extracted from analyses

of deep-inelastic lepton scattering $\ell N \to \bar{\ell} X$ in the region $Q^2 < 0$. Here $\ell = \mu, e$, or ν. This general topic and scaling violations are treated in Sections II and III. Comparisons with data are presented in Section IV. The transverse momentum $\vec{Q}_T$ behavior of the lepton pair production cross-section $d\sigma/d^2\vec{Q}_T\, dQ^2\, dx_F$ is another subject of considerable interest. In QCD the dynamics at high $\vec{Q}_T$ are governed by elementary hard scattering processes analogous to those studied in large $\vec{P}_T$ purely hadronic reactions,[12] such as $h_1 h_2 \to \pi X$. In $h_1 h_2 \to \gamma^* X$, the whole jet (γ^*) is observed experimentally and, therefore, difficulties associated with trigger bias and jet decay are eliminated. This technical advantage of $h_1 h_2 \to \gamma^* X$ has not yet been exploited fully, in part because present data extend only to $|\vec{Q}_T| \lesssim 4$ GeV/c. In the small $\vec{Q}_T$ region, the $\vec{Q}_T$ dependence is influenced by soft-gluon emission processes, by non-perturbative and by bound state effects. While complicating the comparisons of data with calculations of first-order perturbative QCD processes, the physics of these soft-gluon, bound state and non-perturbative effects is of interest in its own right. I discuss transverse momentum distributions and their moments in Section V.

A general conclusion regarding QCD which emerges from comparisons with data is one of rough consistency. There are no glaring failures in regions of phase space where calculations should apply. However, the theory is not being "tested". Important calculations have yet to be made of the size and kinematic variation of non-leading, higher order corrections ($\propto 1/\log Q^2$, $1/Q^2$, ...) before one can be satisfied with the general agreement of theory with the magnitude and with the x_F and M variations of $d^2\sigma/dM\, dx_F$. For Q_T spectra, these objections are compounded by further

questions concerning the applicability of perturbative QCD in the small $\vec{Q}_T$ region ($\vec{Q}_T^2 << Q^2$).

In this review, I attempt to survey the present situation in the phenomenology of massive lepton pair production, enumerating some unresolved issues and points of contention.

II. The Classical Drell-Yan Model and Its Problems

As a point of departure, I begin with the classical Drell-Yan approach.[1] The physical process is sketched in Fig. 1. We imagine that there is a known probability $q_i(x_a, \vec{k}_{Ta})$ for finding a quark of flavor i among the constituents of incident hadron a; this quark carries the fraction x_a ($x_a > 0$) of the longitudinal momentum of hadron a, as well as transverse momentum $\vec{k}_{Ta}$. Likewise, $\bar{q}_i(x_a,\vec{k}_{Tb})$ is the probability for finding an antiquark of flavor j. Later, these functions will be generalized to include explicit Q^2 dependence. In the classical parton model they do not depend on Q^2. In the parton model, the distributions in $\vec{k}_{Ta}$ and $\vec{k}_{Tb}$ are also understood to be sharply limited to small energy independent values, with $\langle k_T \rangle \simeq 300$ MeV. The classical Drell-Yan cross-section for $h_a h_b \to \ell^+\ell^- X$ is then

$$\frac{Q^2\, d\sigma^{ab}}{dQ^2\, dx_L\, d^2\vec{Q}_T\, d\cos\theta^*} = \frac{\pi\alpha^2}{2} \int d^2\vec{k}_{Ta}\, dx_a\, d^2\vec{k}_{Tb}\, dx_b \qquad (1)$$

$$\frac{1}{3}\sum_i e_i^2 \left[q_i(x_a,\vec{k}_{Ta})\ \bar{q}_i(x_b,\vec{k}_{Tb}) + \bar{q}_i(x_a,\vec{k}_{Ta})\ q_i(x_b,\vec{k}_{Tb}) \right]$$

$$(1+\cos^2\theta^*)\ \delta^{(2)}(\vec{Q}_T - \vec{k}_{Ta} - \vec{k}_{Tb})\ \delta(x_L - x_a - x_b)\ \delta(Q^2 - x_a x_b s)\ .$$

In the $\ell^+\ell^-$ rest-frame, θ^* is the polar angle of a lepton ℓ with respect to the axis defined by the collinear $q\bar{q}$ system; e_i is the fractional

quark charge. Displayed explicitly in the denominator of Eq. (1) is a factor 3 representing the three colors of quarks; the distributions q and $\bar{q}$ are summed over the color index.

The expression on the right hand side of Eq. (1) is the leading contribution in the $Q^2 \to \infty$ limit. Terms have been dropped which are proportional to Q^{-2} relative to the result shown. In some cases, these Q^{-2} terms may be shown to have a different dependence on, e.g., x_F and $\cos\theta^*$. For example, at large x_F in $\pi p \to \mu\bar{\mu}X$, $d\sigma/d\cos\theta^*$ is predicted[13] to vary as $\sin^2\theta^*$, instead of the oft-quoted $(1+\cos^2\theta^*)$. I restrict my attention in this paper to values of the lepton pair mass $M > 4$ GeV, in order to exclude the J/ψ resonance region, and to ensure that conditions are satisfied for valid application of the impulse approximation. The Υ region $9.0 < M < 10.5$ GeV should also be excluded.

There are at least two phenomena which require our going beyond the basic model. These are the observed relatively large values[4-9] of $\langle Q_T \rangle$ in $hh \to \mu\bar{\mu}X$, and the scaling violations in $q(x,Q^2)$ (i.e., explicit Q^2 dependence at fixed x) observed in deep-inelastic μ and ν scattering.[14-17] Within the context of QCD both phenomena are interpreted as manifestations of gluonic radiative processes.

1. Q_T effects

The basic amplitude A_μ represented by Fig. 1 is not manifestly gauge invariant ($A_\mu \cdot Q^\mu \neq 0$) if the quark and/or antiquark are off-shell.[1,18] For example, if we consider quark a to be off-shell with b on-shell, the amplitude will contain a factor $\not{q}_a \gamma_\mu u(q_b)$. Therefore, $A_\mu \cdot Q^\mu \propto q_a^2$, where q_a^μ is the four-vector momentum of quark a. Using energy-momentum conservation for $h_a \to q_a + X_a$, we may easily show that

$$q_a^2 = \frac{-k_{Ta}^2}{(1-x_a)} + \ldots \qquad (2)$$

The mass terms (...) ignored in Eq. (2) are inconsequential for the present discussion. If k_{Ta}^2 is very small ($\langle k_{Ta} \rangle \simeq 300$ MeV), as is required in the classical parton model, and if x_a is not near 1, then q_a^2 is negligible with respect to Q^2, and the classical model ought to be applicable. However, it is observed experimentally[4] that $\langle Q_T^2 \rangle \simeq 1.8$ GeV^2 for $5 < M_{\mu\mu} < 10$ GeV at $p_{lab} = 400$ GeV/c. Moreover, a comparison of FNAL and ISR data, as shown in Fig. 2, suggests that $\langle Q_T^2 \rangle$ increases with p_{lab}, perhaps as fast as $\langle Q_T^2 \rangle \propto s$. If we attempt to explain these effects entirely with intrinsic quark transverse momenta, we deduce that $\langle k_{Ta}^2 \rangle \simeq \frac{1}{2} \langle Q_T^2 \rangle \simeq 1$ GeV^2 at 400 GeV^2. Thus, $1 \leq |q_a^2| \leq 10$ GeV^2 for $0 \leq x_a \leq 0.9$. This is an unacceptably large violation of gauge invariance. While non-asymptotic kinematic effects should play some role, the increase of $\langle Q_T^2 \rangle$ with s at fixed Q^2/s also cannot be explained purely with intrinsic quark and antiquark transverse momenta. Because $\langle k_{Ta}^2 \rangle$ depends only on x_a, $\langle Q_T^2 \rangle$ should in turn be independent of s at fixed Q^2/s.

2. Scaling violations

Although there is some controversy regarding the detailed interpretation of the results,[19,20] high energy data on deep-inelastic muon and neutrino scattering[14-17] cannot be described with scaling structure functions, $q(x)$ and $\bar{q}(x)$. It is "natural" to interpret the data instead in terms of non-scaling distributions $q(x,Q^2)$ and $\bar{q}(x,Q^2)$. In deep-inelastic scattering these functions are measured in the time-like $Q^2 < 0$ region. Strong theoretical guidance is necessary in order to relate these distributions obtained in the $Q^2 < 0$ deep-inelastic region

to those which are appropriate in the time-like $Q^2 > 0$ region for $hh \to \mu\bar{\mu}X$ in Eq. (1). Without such guidance, Eq. (1) has little predictive power, since it is unclear what meaning to attach to the functions $q(x)$ and $\bar{q}(x)$ if they are unrelated to those for deep inelastic scattering. QCD supplies a prescription for connecting the $Q^2 < 0$ and $Q^2 > 0$ regions.

In Section III, I describe QCD modifications to the classical Drell-Yan pciture.

III. Beyond the Classical Model

The incident hadrons may be imagined to be beams of quarks, antiquarks, and gluons. At a somewhat lower level of resolution, e.g., smaller Q^2, the beams also contain "bound" constituents, such as virtual mesons ($q\bar{q}$) and diquarks (qq). For the moment, I assume that the only initial constituents are the quarks, antiquarks, and gluons, and that these constituents are free, unbound. Later it will be essential to reexamine this assumption and to ask to what extent the neglect of bound state effects and substructure ($q\bar{q}$,qq,...) affects our conclusions.

There are many ways in which a massive γ^* may be produced from the interaction of the initial constituents. In QCD, or in any field theory of interacting constituents, we may draw an entire series of diagrams, ordered according to the strong coupling constant α_s. Some of these are illustrated in Fig. 3, beginning with the basic zero order diagram $q\bar{q} \to \gamma^*$. In first order in α_s, there is an <u>initial</u> gluon set ("Compton scattering") Figs. 3(b) and (c), for which the subprocess $qG \to \gamma^* q$ is driven by the gluon distribution in one of the initial hadrons, as well as the <u>final</u> gluon set ("two body annihilation") Figs. 3(d) and (e) in

which a gluon is radiated into the final state $q\bar{q} \to G\gamma^*$. The initial constituents q, $\bar{q}$, or G in Fig. 3 are all intended to be on-shell, although for formal reasons one often assigns each a small off-shell value of $p^2 < 0$. Additional gluons may be radiated from the initial or final constituent lines in Fig. 3, leading to graphs of higher order in α_s.

The series of graphs in Fig. 3 suggests that the cross-section for $h_a h_a \to \gamma^* X$ receives contributions from four types of terms, expressed symbolically as

$$\begin{aligned}
\sigma_{ab\to\gamma^*X} &= \int q_a(x_a)\ \bar{q}_b(x_b)\ \sigma_{q\bar{q}\to\gamma^*X_1} \\
&+ \alpha_s \int \left[q_a(x_a)\ G_b(x_b) + \bar{q}_a(x_a)\ G_b(x_b) \right] \sigma_{qG\to\gamma^*X_2} \\
&+ \alpha_s^2 \int q_a(x_a)\ q_b(x_b)\ \sigma_{qq\to\gamma^*X_3} \\
&+ \alpha_s^2 \int G_a(x_a)\ G_b(x_b)\ \sigma_{GG\to\gamma^*X_4} \\
&+ (a \leftrightarrow b) \qquad (3)
\end{aligned}$$

Here the distributions $q(x), \bar{q}(x)$, and $G(x)$ describe the quark, antiquark, and gluon densities in the initial states. In Eq. (3), the symbols X_i represent states of various multiplicities of quarks, antiquarks, and gluons.

Graphs which are of high order in α_s cannot be dismissed. Their contribution to the integrated cross-section $d\sigma/dQ^2$ may be shown to be proportional to $(\alpha_s \log Q^2)^n$. Even if $\alpha_s \propto 1/\log Q^2$, all terms in the series are of comparable magnitude. In nucleon-nucleon collisions, it

may be imagined that the $O(\alpha_s^2)$ term with $qq \to qq\gamma^*$, Fig. 3(f), would be more important than the simple annihilation term $q\bar{q} \to \gamma^*$ which feeds on the small sea in the nucleon. Fortunately, techniques have been devised to "sum" the series of terms in α_s, at least in the leading logarithmic approximation to each order.[21-23] The procedure parallels that employed in deep inelastic processes,[20] although with less rigor. The general conclusion is that in QCD, the Drell-Yan cross-section, Eq. (1), integrated over $\vec{Q}_T$, should still be valid, except for the replacement of the scaling $q(x)$ and $\bar{q}(x)$ structure functions with scale-noninvariant forms $q^{DY}(x,Q^2)$ and $\bar{q}^{DY}(x,Q^2)$. This replacement takes into account the leading logarithmic contributions of all terms in the series in α_s. Moreover, analyses show that the functions $q^{DY}(x,Q^2)$ and $\bar{q}^{DY}(x,Q^2)$ should be identical to the functions $q^{DIS}(x,Q^2)$ and $\bar{q}^{DIS}(x,Q^2)$ measured in deep-inelastic electroproduction and in neutrino scattering.

The statements made above are true only to leading order in $\log Q^2$. Even when Q^2 dependent structure functions are used, one expects QCD corrections to the Drell-Yan prediction which are proportional to $1/\log Q^2$. In order α_s, these arise from the "constant" terms which remain after the dominant $\log Q^2$ divergent piece is removed and absorbed into the renormalized structure functions. It is important to calculate explicitly the expected size and kinematic variation (with Q^2, s, x_F, y) of these correction terms, since $1/\log Q^2$ is not small for values of Q^2 now accessible experimentally. As is well known, QCD fits to scale violating effects in DIS depend sensitively on the controversial scale parameter Λ; differences in Λ are $1/\log Q^2$ effects. A few groups have undertaken an estimate of the $1/\log Q^2$ corrections in $hh \to \mu\mu X$. Effects as large as

100% are found[24] for values of s and Q^2 typical of present experiments. The corrections are sizeable for both $\bar{p}N$ and pN processes, and are therefore not a peculiarity of the small sea distribution in the nucleon. The large size of the $1/\log Q^2$ corrections calls perturbation theory into question, for, if $1/\log Q^2$ terms are of order 100%, what of the neglected $(1/\log Q^2)^2$ terms? In Section IV.2, I show that present data are also consistent with large deviations from the leading order Drell-Yan expression.

The leading $(\log Q^2)^n$ terms in $hh \to \mu\bar{\mu}X$ arise after an integration over $\vec{Q}_T$, and, thus, the analysis described here is relevant only for the cross-section integrated over $\vec{Q}_T$, i.e., for $d\sigma/dQ^2\, dx_F$. I will return to a discussion of $\vec{Q}_T$ effects in QCD in Section V.

In the paragraphs above, I discussed hadronic collisions as if they are really collisions of free, unbound, on-shell, colored elementary constituents. However, free quarks and gluons do not exist, and there may well be important physical effects in $hh \to \mu\bar{\mu}X$ associated with the fact that constituents are bound in color-singlet hadronic wavefunctions. Binding implies, among other things, that the constituents may be far off-shell in some kinematic regions.

Although the full bound state problem is one which is inherently nonperturbative, it has been argued[25] that QCD perturbation theory can be employed for calculations of the "hard-part" of bound-state effects, including, for example, the behavior of structure functions as $x \to 1$. This leads to the possibility of going beyond the simple probabilistic, factorizing form of Eq. (1), and of looking for physical correlations between effects traditionally separated into the "structure function"

and "elementary constituent cross-section" factors in Eqs. (1) and (3). While introducing new complexities, the bound state effects also open a broader range of possibilities for testing QCD.

One example of the above ideas is the recent calculation[13] of the pion structure function, based on the diagrams shown in Fig. 4. It was shown that there are two contributions to the structure function, and to the Drell-Yan cross-section for $\pi N \to \mu\bar{\mu}X$, one associated with transversely polarized γ^* and a second, dominant at large x_F, associated with longitudinally polarized γ^*. At large x, where the antiquark in the pion carries most of the momentum of the incident meson, the dominance of the longitudinal cross-section reflects the antiquark's "memory" of its origins in an integer spin boson.

A different aspect of the bound-state problem is emphasized by Blankenbecler and collaborators.[18,26,27] They argue that at small Q^2 and Q_T^2, the important hadronic constituents are those associated with the large distance structure of the hadron, namely, the light mesons. Thus, as Q^2 or Q_T^2 grows, corresponding to probing to smaller distances, the dominant constituent scattering processes should change gradually from meson-meson processes, to meson-quark and diquark-antiquark processes, and, finally, at the highest Q^2, to quark-gluon and quark-antiquark processes. At modest values of Q^2 and/or Q_T^2, one should explicitly include contributions to the cross-section $d\sigma/dQ^2\, dQ_T^2$ associated with, e.g., the meson-quark subprocess.[18]

Finally, I should mention the possibility that non-trivial, non-perturbative effects may invalidate the simple factorizing form of Eq. (1), and of all the higher order QCD corrections to it. These effects are illustrated by, but not limited to, the initial state and final-state

interactions[28] sketched in Fig. 5. Instanton effects[29] have been suggested as a possibly large non-factorizing source of deviations from the Drell-Yan formula, but have not yet been shown to be numerically large enough to warrant concern.

I have done little more here than to advocate the desirability of going beyond elementary field calculations to include bound state effects properly. It is a problem of more than prosaic interest in many respects, for example, in attempts to describe the $\vec{Q}_T$ distribution (cf., Section V). In deep inelastic scattering as well as in massive lepton pair production, physical effects associated with the bound state origins of the initial constituents are no less interesting, nor less important in the presently explored interval of Q^2, than the much explored logarithmic effects due to gluonic radiative corrections.[20]

IV. Comparisons with Experiment

In the previous Section I surveyed some of the theoretical ideas of interest in connection with the cross section for $h_a h_b \to \mu\bar{\mu}X$. Here I shall adopt the simplest view, viz., that the cross-section integrated over $\vec{Q}_T$ is predicted exactly by the Drell-Yan formula, Eq. (1), with only one modification, which is the use of Q^2 dependent structure functions $q(x, |Q^2|)$ extracted from data on deep-inelastic lepton scattering (DIS). My aim is to compare the resulting "predictions" with data on $hh \to \mu\bar{\mu}X$ to see to what extent this simple view is consistent with experiment. I focus on the absolute yield and on the s, M, and x_F variations of $d\sigma/dM\, dx_F$. There are other predictions, of course, but these have been reviewed adequately elsewhere.[2,3]

1. Valence-valence processes

(a) $\bar{p}p$. In many respects, the $\bar{p}p$ (or $\bar{p}N$) process is ideal. In the approach I have adopted the cross-section $\sigma \propto \bar{q}_{\bar{p}}(x_a,Q^2)\ q_p(x_b,Q^2) = q_p(x_a,Q^2)\ q_p(x_b,Q^2)$ is specified entirely in terms of quark structure functions which can be extracted reasonably reliably from DIS. However, there are as yet no high energy data on $\bar{p}N \to \mu\bar{\mu}X$.

(b) πN. The process $\pi^- N \to \mu\bar{\mu}X$ has recently been investigated in detail at high energies.[9-11] According to the model, the cross section is a sum of two pieces, $\sigma = q_\pi \bar{q}_N + \bar{q}_\pi q_N$. Since the antiquark content $\bar{q}_N$ of the nucleon is relatively small, the cross-section is represented to first approximation by the second term: $\bar{q}_\pi(x_\pi)\ q_N(x_N)$. More precisely,

$$\sigma \propto \bar{q}_\pi(x_\pi,Q^2)\left[\frac{4}{9}\, x_N\, u_N(x_N,Q^2) + \frac{1}{9}\, x_N\, \bar{d}_N(x_N,Q^2)\right] \quad . \qquad (4)$$

If we adopt the values of $u_N(x_N,Q^2)$ and $\bar{d}_N(x_N,Q^2)$ determined in DIS experiments, Eq. (4) can be used to determine $\bar{q}_\pi(x,Q^2)$ from the data. However, there is even more content to Eq. (4). Recognizing that the logarithmic Q^2 variation predicted by QCD is relatively mild for $Q^2 \gtrsim 10\ \mathrm{GeV}^2$ (i.e., above the J/ψ peaks), we may begin by ignoring it in Eq. (4). Then, the two kinematic variables x_π and x_N in Eq. (4) may be reexpressed in terms of the two observables $x_F \approx x_\pi - x_N$ and $Q^2 = s x_\pi x_N$. The manner in which the observed non-zero value of Q_T^2 is handled leads to some uncertainty in the resolution of these equations for x_π and x_N in terms of Q^2 and x_F, but the results I shall describe are not affected in any meaningful way.

A check was made by the Chicago-Princeton group[9] that the dependence of their data on x_π and x_N agrees with the factorization property in

Eq. (4); i.e., $\sigma \propto f_1(x_\pi) f_2(x_N)$. The agreement is a verification that one dominant production mechanism is at work, and that its effects are at least consistent with the factorization property of Eqs. (1) and (4). Next, the functional dependences of $\bar{q}_\pi(x_\pi)$ on x_π and of $q_N(x_N)$ on x_N were extracted from the data. A meaningful question is whether the x_N dependence of $q_N(x_N)$ from $\pi N \to \mu\bar{\mu}X$ is consistent with that seen in deep inelastic reactions. This has also been answered in the affirmative by the Chicago-Princeton collaboration, in the limited range $0.05 < x_N < 0.3$ accessible in their experiment, and for $\langle Q^2 \rangle \approx 25$ GeV^2. Only the shape can be checked, of course, not the absolute normalization of $q_N(x_N)$. Finally, adopting the absolute normalization of $q_N(x_N)$ from DIS data, the Chicago-Princeton group[9] used their data to extract an absolutely normalized function $x_\pi \bar{q}_\pi(x_\pi)$ for $0.3 < x_\pi < 0.95$. Their results are shown in Fig. 6; they have been fitted to the form

$$x\bar{q}_\pi(x) = A(1-x)^p \qquad (5)$$

with $p = 1.01 \pm 0.05$ and $A = 0.52 \pm 0.03$, for $\langle Q^2 \rangle \approx 25$ GeV^2.

The results of the Chicago-Princeton group are in good accord with the parton model, with color, but QCD cannot be said to play much of a role. The shape (x_N dependence) of $q_N(x_N)$ seems to be the same in DIS and in $\pi p \to \mu\bar{\mu}X$ for $0.05 < x_N < 0.3$ and $\langle Q^2 \rangle \approx 25$ GeV^2. Second, the integral $\int x\,\bar{q}_\pi(x)\,dx \simeq 0.20$ shows that about 40% of the pion's momentum is carried by quarks and antiquarks, as seems "reasonable". If there were no color factor in Eq. (1), this fraction would be reduced to $40/3 \approx 14\%$, which seems clearly wrong. Thus, the color factor is supported. Finally, the x_π dependence of $x_\pi q_\pi(x_\pi)$ is very close to the parton model/constituent counting rules prediction of $(1-x)^1$, derived, however, for <u>spinless</u> quarks.[30]

This last point deserves some discussion. The fact that the quarks carry spin 1/2 seems well established by the fact that the angular distribution $d\sigma/d\cos\theta^*$ is observed by the Chicago-Princeton group to be approximately of the form $(1+\alpha\cos^2\theta^*)$ with $\alpha \simeq 1$. Spinless quarks (or a mechanism[27] such as $\pi\pi \to \gamma^* \to \mu\bar{\mu}$) would require $d\sigma/d\cos\theta^* \propto \sin^2\theta^*$ because the γ^* is then necessarily longitudinally polarized. However, spin 1/2 quarks also lead to an <u>even</u> power behavior[31] of $xq_\pi(x)$ as $x \to 1$: $(1-x)^2$ or $(1-x)^0$, not $(1-x)^1$. It seems, therefore, that there is an inconsistency between the observations of $d\sigma/d\cos\theta^* \propto (1+\cos^2\theta^*)$ and $xq_\pi(x) \propto (1-x)^1$. This paradox may be resolved by a more careful study of the x_F, Q^2, and $\cos\theta^*$ dependences of the data, as described below. The $(1-x)^1$ result may be regarded as a "spin-averaged" answer.

Within a specific QCD representation of the behavior of the (spin 1/2) quarks in a pion, it was shown recently[13] that the structure function should have the form

$$xq_\pi(x) \propto (1-x)^2 + \frac{2}{9}\frac{c}{Q^2}(1-x)^0 \quad . \qquad (6)$$

Here c is a constant of order 1 GeV^2. For $\langle Q^2\rangle \simeq 25$ GeV^2, as in the data, the sum of terms in Eq. (6) may easily mimic the observed $(1-x)^1$ behavior. It was further shown that the scaling piece, $(1-x)^2$, in Eq. (6) is associated with transversely polarized γ^*'s and thus with a $(1+\cos^2\theta^*)$ angular distribution, whereas the non-scaling portion $(1-x)^0/Q^2$ is tied to longitudinally polarized γ^*'s and therefore to a $\sin^2\theta^*$ distribution. In the data, the angular distribution is weighted heavily by events with small values of x_F (and hence of x_π), and therefore the $(1+\cos^2\theta^*)$ term dominates. If events are selected with $x_F \gtrsim 0.7$, the effects of the non-scaling $(1-x)^0\ Q^{-2}\ \sin^2\theta^*$ term should be enhanced. It would be instructive to

verify whether the correlated x_F, Q^2, and $\cos^2\theta^*$ dependences of the data can be described successfully with forms suggested in Ref. 13. Verification would confirm that bound state effects and structure functions at large x can be understood in some detail in a QCD framework. Note that Eq. (6) also implies a strong violation of scaling in πN processes (i.e., $M^4 d\sigma/dM^2 \neq f(M/\sqrt{s})$) at moderate value of s.

2. Valence-ocean processes

The processes most accessible to experimental investigation are $pp \to \mu\bar{\mu}X$ and $pN \to \mu\bar{\mu}X$ for which the basic interaction is the annihilation of a (valence) quark from one nucleon with an antiquark from the sea in the other nucleon:

$$\sigma \propto q_p(x_p)\ \bar{q}_N(x_N) + \bar{q}_p(x_p)\ q_N(x_N) \quad . \tag{7}$$

Because high energy data, with values of $Q^2 = M^2_{\mu\mu}$ substantially above the J/ψ resonance region, are available at several different energies, a check can be made of the classical scaling relation embodied in Eq. (1): $M^4 d\sigma/dM^2 = f(M/\sqrt{s})$. Attempts can also be made to identify the deviations from exact scaling which are demanded by QCD gluonic radiation graphs. In addition to these issues of scaling and its violation, it is interesting to compare the ocean $\bar{q}_N(x)$ distribution determined from data on $pN \to \mu\bar{\mu}X$ (via the Drell-Yan Eq. (1)) with that determined from deep-inelastic neutrino processes.

(a) Scaling. If perfect scaling holds, as implied by Eq. (1) with structure functions independent of Q^2, then the quantity $sd^2\sigma/d\sqrt{\tau}\,dy$ should be a function only of the ratio $\tau = M^2/s$ and of the lepton pair rapidity y. Using their data from pN processes at 200, 200, and 400 GeV/c, the Columbia-Fermilab-Stony Brook collaboration[4] tested this prediction

at $y \approx 0.2$, the only value of y at which the experimental acceptance permits a comparison of data at different energies. The results are shown in Fig. 7. Scaling is observed to hold to within 20% at $y \approx 0.2$ for $0.2 < M/\sqrt{s} < 0.5$.

This observation of scaling at the 20% level is not inconsistent with the scaling violations inherent in QCD.[32] In the theory, and in DIS data, the pattern of scaling violations is such that distribution functions have a "cross-over" point near $x = 0.2$. For $x < 0.2$, structure functions increase in magnitude as Q^2 grows, whereas for $x > 0.2$ they decrease. The rate of change is only logarithmic in Q^2. In $pN \to \mu\bar{\mu}X$, $x_F = 0$ implies $x_q = x_{\bar{q}} = M/\sqrt{s}$. Therefore, for $y \sim 0$ and $M/\sqrt{s} \sim 0.2$, QCD provides essentially no deviation from exact scaling. For $y \sim 0$ and $M/\sqrt{s} > 0.2$, a slow (logarithmic) decrease with s of $sd^2\sigma/d\sqrt{\tau}\, dy$ should be observed. For $y \simeq 0$ and $M/\sqrt{s} < 0.2$ a slow growth is predicted. These qualitative expectations are as consistent with the data in Fig. 7 as is the statement of perfect scaling. The lever arm in s in the Fermilab energy range is too small to yield any appreciable deviations from scaling unless x_F and $M/\sqrt{s}$ are large.

In an attempt to increase the lever arm, it is desirable to compare data from Fermilab with results from the CERN-ISR. However, this endeavor is unsatisfactory because the ranges of $M/\sqrt{s}$ do not overlap. One comparison is shown in Fig. 8: ISR results are clustered in the region $M/\sqrt{s} < 0.2$, whereas the Fermilab data populate $M/\sqrt{s} > 0.2$. The Fermilab results may not be extended to lower $M/\sqrt{s}$ because of the J/ψ resonance effects. To extend the ISR results to higher values of $M/\sqrt{s}$ would require data at large values of M, where rates are punishingly low.

(b) University of the ocean? If we adopt quark distribution functions determined from DIS experiments, the Fermilab data on $pN \to \mu\bar{\mu}X$ can be used to extract an absolutely normalized sea quark spectrum $\bar{q}_N(x,Q^2)$ for $16 \lesssim Q^2 \lesssim 200$ GeV^2 and $0.2 < x < 0.5$. It is interesting to compare this sea with that determined from deep-inelastic neutrino scattering. As discussed in Section III, if Q^{-2} and $1/\log Q^2$ corrections to the Drell-Yan equation are unimportant, QCD requires these two ocean spectra to be identical at the same values of x and Q^2.

In Fig. 9, I compare ocean spectra extracted from the Columbia-Fermilab-Stony-Brook data[4] on $pN \to \mu\bar{\mu}X$, and from the CERN-Dortmund-Heidelberg-Saclay data[14] on $\nu N \to \mu X$ and $\bar{\nu}N \to \mu X$. Some comments about the treatment of the data are in order before conclusions may be drawn. In the pN experiment, the contributions of the strange and charm quark seas are presumably entirely negligible; they have been neglected in the fit to the data. For the results shown, it was assumed in the fit that $\bar{u}(x,Q^2) = \bar{d}(x,Q^2)$. However, if one assumes $\bar{u} \neq \bar{d}$ (e.g., $\bar{u} \propto (1-x)^3\bar{d}$), the results for the average quantity shown in Fig. 9 do not change in any significant way. Note that values of x and Q^2 in the pN results are correlated: at $x_F = 0$, where the data are concentrated, $Q^2 = sx^2$. To break this coupling, and thus to extend the results to lower x, one needs data over a range of values of x_F. The pN points may be fitted to the simple form

$$\frac{1}{2}\, x(\bar{u} + \bar{d}) \;=\; A(1-x)^B \quad , \tag{8}$$

with $A = 0.56 \pm 0.04$, and $B = 9 \pm 1$. In this fit, the values of A and B are taken to be independent of Q^2, whereas in a QCD approach one would expect both to change logarithmically with Q^2. The meager data do not

yet warrant more sophistication, but it should not be forgotten that A and B are appropriate for a wide band in Q^2: $20 < Q^2 < 200$.

Even more discussion of the νN results is necessary. The points shown were extracted from Fig. 18 of Ref. 14, and that paper should be consulted for details of the data analysis. Presented in Fig. 18 of Ref. 14 are values of the ratio

$$\frac{x\bar{q}(x) + x\bar{s}(x)}{\int (xq(x) + x\bar{q}(x))\, dx} \quad , \tag{9}$$

where $\bar{q}(x) = \bar{u}(x) + \bar{d}(x) + \bar{s}(x)$. In the text of Ref. 14 it is stated that $\int F_2\, dx = \int (x\, q(x) + x\bar{q}(x))\, dx = 0.44 \pm 0.02$ for $30 < E_\nu < 90$ GeV, and $\int F_2\, dx = 0.45 \pm 0.03$ for $90 < E_\nu < 200$ GeV. The portion of the strange sea may be estimated from dimuon production in neutrino interactions:[33]

$$\frac{\int x\bar{s}(x)\, dx}{\int (xq(x) + x\bar{q}(x))\, dx} = 0.025 \pm 0.01 \quad . \tag{10}$$

Moreover, in Ref. 14 it is determined that

$$\frac{\int (x\bar{q} + x\bar{s})\, dx}{\int (xq + x\bar{q})\, dx} = 0.16 \pm 0.01 \quad . \tag{11}$$

Combining Eqs. (10) and (11), I find that

$$\left[\bar{u}(x) + \bar{d}(x)\right] \simeq 0.688\left[\bar{q}(x) + \bar{s}(x)\right] \quad . \tag{12}$$

I used this last expression in translating points from Fig. 18 of Ref. 14 to my Fig. 9. In Ref. 14, a fit is made of the form

$$x\left[\bar{q}(x) + \bar{s}(x)\right] \propto c(1-x)^d \quad , \tag{13}$$

with $d = 6.5 \pm 0.5$. I show this form in Fig. 9, with my determination of normalization coefficient $c = 0.18$, obtained through the same manipulations I described above.

The neutrino data provide a representation of the sea for $0.05 < x < 0.25$ and $5 \lesssim Q^2 \lesssim 20$ GeV^2. This kinematic range overlaps that of the pN data only for x near 0.2 and $Q^2 \simeq 20$ GeV^2. In this region of overlap, the magnitude of the sea determined in νN processes is at most one-half that observed in $pN \to \mu\bar{\mu}X$. If the drastic assumption is made that the strange sea can be ignored completely in the νN data, the νN points in Fig. 9 would be moved up by a factor of 1.5, leaving them still at a level of at most 75% of the pN points near $x = 0.2$.

The differences in the parameters of the fits shown in Fig. 9 are not necessarily significant since the fits are done in different x and Q^2 ranges. However, near $x = 0.2$ and $Q^2 = 20$ GeV^2 it is evident that the oceans extracted from νN and pN data do not agree. The effective sea distributions are not universal.

Can one explain this discrepancy? Obviously the data may not be sufficiently precise, but a factor of two seems too much to assign to purely experimental problems. It is possible that the (valence) quark structure function used in the analysis of $pN \to \mu\bar{\mu}X$ is incorrect, biasing the final results for the sea distribution. I have not checked this point, but, again the required factor of two is unlikely. Part of the discrepancy between the ocean spectra in Fig. 9 may be explained with the type of Q^2 variation which QCD provides. As Q^2 grows, the magnitude of the sea is predicted to increase at small x; the effective power p in a fit of the form $(1-x)^p$ should also grow. These two effects are consistent with the trends indicated in Fig. 9. However, again, the magnitude of the discrepancy seen in Fig. 9 is too great. One obvious explanation is that the discrepancy should be attributed to neglect of the

$1/\log Q^2$ (or $1/Q^2$) QCD correction terms discussed in Section III. Published estimates[24] suggest that the first order $1/\log Q^2$ effects may indeed be as large as 100%. If the comparison shown in Fig. 8 is substantiated by further experimental analyses, it is evident that QCD calculations must be pushed to higher order in all processes, including a quantitative treatment of all $1/\log Q^2$ (and $1/Q^2$) effects.

V. Transverse Momentum Spectra

As mentioned in Section II, the fact that $\langle Q_T \rangle$ is relatively large and seems to be an increasing function of s requires a treatment of transverse momentum spectra which goes beyond the classical parton model. The data cannot be explained satisfactorily simply by assigning quarks and antiquarks an "intrinsic" non-perturbative transverse momentum spectrum, although such a contribution is surely a part of the full picture. In a first-order perturbative QCD approach,[3,34,35] the large Q_T tail of the Q_T distribution in $hh \to \mu\mu X$ is generated by the $O(\alpha_s)$ graphs shown in Fig. 10. These QCD contributions can explain naturally the growth of $\langle Q_T \rangle$ with s. However, since data now extend only to $|\vec{Q}_T| \lesssim 4$ GeV/c, there is not a large region in Q_T in which we are justified in comparing the model with present data on $d\sigma/d^2\vec{Q}_T$. The region $Q_T < 1$ GeV/c is certainly outside the scope of the perturbative QCD approach, and even the intermediate region $Q_T \lesssim 4$ GeV/c seems to be below the range of applicability of the simple $O(\alpha_s)$ approach. I will describe first what has been done with the $O(\alpha_s)$ approach and then discuss modifications,[36-38] as well as other approaches.[18,39,40] In the "successful" fits to data on the transverse momentum distribution, success is achieved largely

through the introduction of small Q_T effects which have little or nothing to do with QCD.

1. Comparison with $O(\alpha_s)$ QCD contributions

The distribution $Ed\sigma/d^3\vec{Q}$ which I obtained from the $O(\alpha_s)$ QCD graphs is shown in Fig. 11 as a function of Q_T for $pN \to \mu\bar{\mu}X$ at 400 GeV/c, $7 < M_{\mu\mu} < 8$ GeV, and $y = 0$. Shown for comparison are data from the Columbia-Fermilab-Stony Brook collaboration. Details of the calculation may be found in Ref. 3. Simple QCD cross-sections obtained from the graphs in Fig. 10 are convoluted with quark, antiquark and gluon densities in the initial hadrons. The initial and final quarks and gluons are taken to be massless and on-shell. The initial quark structure functions are obtained from data on DIS. The initial antiquark distribution is deduced from my fit[3] to the cross-section $d\sigma/dMdy$ for $pN \to \mu\bar{\mu}X$, integrated over $\vec{Q}_T$. For the initial gluon density, I use

$$xG(x) = \frac{1}{2}(p+1)(1-x)^p \qquad (14)$$

with $p = 6$. I set the strong coupling "constant" $\alpha_s = 0.3$. I ignore Q^2 dependence in α_s and in the structure functions. To first order in α_s this neglect is immaterial; corrections are of higher order in α_s.

Evident in Fig. 11 is the divergence ($\propto Q_T^{-2}$) associated with the "mass singularity" in the $O(\alpha_s)$ amplitudes when the exchanged quark goes on-shell. The large tail of the distribution is controlled by the large x behavior of the quark, antiquark, and gluon densities in the initial hadrons. The "Compton" ($qG \to \gamma^* q$) contribution in Fig. 11 falls off less rapidly with Q_T than the annihilation ($q\bar{q} \to \gamma^* G$) contribution because in nucleons the initial gluons are harder (have larger $\langle x \rangle$) than

the initial antiquarks. In $\bar{p}N$ processes, roles are reversed, and the large Q_T behavior is controlled by the two body annihilation process $q\bar{q} \to \gamma^* G$. Therefore, in pN reactions, the large Q_T γ^* is balanced in Q_T by a quark jet, whereas in $\bar{p}N$ (and $\pi^- N$) reactions, the large Q_T γ^* is balanced by a gluon jet. This suggests that in order to isolate gluon jets it would be useful to trigger on a large Q_T γ^* produced in $\bar{p}N$ or $\pi^- N$ reactions.

In Fig. 11, I have sketched a wall at $Q_T = 1$ GeV/c below which the theory is clearly inapplicable. Below $Q_T = 1$ GeV/c, perturbation theory breaks down, and various non-perturbative, bound state, soft gluon, coherence, color shielding, and other effects surely dominate the behavior of the Q_T spectrum. However, the comparison of theory and data in Fig. 11 suggests that the $O(\alpha_s)$ QCD result is inadequate even in the intermediate region $4 > Q_T > 2$ GeV/c. Two aspects of the discrepancy may be noticed: the theory falls below the data by a factor of 2 in absolute normalization, and the concavities do not seem to match well. The implementation of various schemes for removing the Q_T^{-2} divergence (such as off-shell kinematics or quark masses) can only worsen the discrepancy in absolute rate. The theoretical yield can be raised only if one adopts unreasonably large values of α_s, or structure functions whose normalization is too large.[41]

2. Beyond $O(\alpha_s)$

Attempts have been made to go beyond the $O(\alpha_s)$ calculation. It is desirable to try to sum contributions to all orders in α_s, at least in the leading logarithm approximation. When only one momentum variable grows in unbounded fashion, as at large Q_T with fixed small Q^2, or at

large Q^2 in DIS with an integral done over Q_T, a summation over leading logarithms to all orders in perturbation theory modifies the classical parton model by the simple replacement of structure functions with scaling violating forms, such as $q(x,\log Q_T^2)$. However, when both Q_T and Q^2 are large, as we require now, the presence of the two large mass scales complicates the analysis. Nevertheless, as a result of summing over leading logarithms, Dokshitzer, Dyakonov, and Troyan[23,36] have succeeded in showing that the lowest order cross-section is modified by a function depending on $\log(Q^2/Q_T^2)$, for $Q_T^2 \ll Q^2$. The higher order gluonic radiation terms result in an effective "form-factor" in Q_T^2. In addition to the limitation $Q_T^2 \ll Q^2$, the DDT answer is also valid only for

$$\frac{\alpha_s(Q_T^2)}{\pi} \log\left(\frac{Q^2}{Q_T^2}\right) \ll 1 \quad , \tag{15}$$

i.e., $Q_T^2 \gg \Lambda Q$, where Λ is the usual scale parameter in QCD. Kajantie and Lindfors[37] compared results obtained in the simple $O(\alpha_s)$ approach with those from the DDT method. Two important qualitative conclusions emerge from their analysis.[37] The DDT result provides the type of concavity of the distribution $d\sigma/dQ_T^2$ which is seen in the data (i.e., as $Q_T \to 0$, the distribution begins to flatten). A second improvement is in the absolute rate, with the DDT curve above the simple $O(\alpha_s)$ result by about a factor of 2, as the data require. No detailed comparisons of the DDT results with data have been published as yet. However, the improvements noted by Kajantie and Lindfords indicate that the DDT method is promising.

An alternative approach for including the effects of soft gluon

emission was proposed recently by Parisi and Petronzio.[38] Their formal results differ from those of DDT, but they also find that incorporation of the soft gluon effects improves the agreement of the Q_T spectrum with data.

3. Higher-twist effects

A different approach to physics in the intermediate Q_T region is based on the constituent interchange model (CIM), or, equivalently "higher-twist" QCD contributions.[39] In the CIM approach, it is stressed that there is important bound or quasi-bound substructure in hadrons, in addition to the "free" quarks, gluons, and antiquarks. Examples are mesonic ($q\bar{q}$) and diquark (qq) constituents of hadrons. Since the virtual mesonic ($q\bar{q}$) substates are colorless, they are presumably relatively long-lived. The scattering of such substates can be shown to yield cross-sections which may overwhelm those from the simple elementary constituent scattering terms in some regions of phase space. In inclusive large p_T hadronic scattering, e.g., $pp \to \pi X$, the CIM contributions provide a cross-section falling like p_T^{-8}, resembling the data more in the region $2 < p_T < 8$ GeV/c than the simple p_T^{-4} contributions.[12] In Fig. 12(a) I illustrate the CIM contributions ($M+q \to \gamma^* q$) to massive γ^* production. The analogous terms for large p_T hadron production are shown in Fig. 12(b).

Detailed studies of the CIM contributions to massive lepton pair production have been made by Blankenbecler and Duong-van,[18] and by others.[40] The absolute rate of the CIM contribution to $pp \to \gamma^* X$ at fixed Q_T is fixed by parameters determined in CIM fits to $pp \to \pi X$ at large p_T. In Fig. 13 I present a comparison of the CIM contribution with the simple $O(\alpha_s)$ QCD results. For $Q_T < 5$ GeV/c, the CIM contribution is larger

than the $O(\alpha_s)$ QCD result. As Q_T grows at fixed Q^2, the CIM cross-section falls as Q_T^{-6} whereas the $O(\alpha_s)$ terms behave as Q_T^{-4}.

The results in Fig. 13 suggest that a proper description of the data on $pp \to \gamma^* X$ in the intermediate Q_T region requires the CIM terms. Away from $Q_T = 0$, the incoherent addition of the CIM and $O(\alpha_s)$ QCD contributions seems to be justified because the flow of color is not identical in the two cases. After the meson M is removed, the remaining hadron is still colorless, whereas after a gluon is removed, the hadronic residue is colored. However, this issue is somewhat clouded since the manner by which color neutrality is restored after constituent scattering is almost never addressed. Another aspect of a (possible) double counting problem has to do with overall normalization, even if incoherence is assumed. The normalization of the initial constituent densities has to be done in a consistent manner.

4. Small Q_T

Regardless of whether one follows the simple $O(\alpha_s)$ QCD approach or the CIM approach, the region $Q_T < 1$ GeV/c requires special treatment. Fits to the data extending into this region have been proposed and, as fits go, they are successful. However, the fits in this region, whether successful or not, have little to do with the basic dynamics of the various approaches.

If the initial and final constituents are massless, the mass-singularity divergence of the cross-section at $Q_T = 0$ is present in both the CIM and QCD approaches. Simple kinematic arguments indicate, however, that the constituents are not massless and not on-shell. For example, if we apply energy and momentum conservation constraints to

the vertex $h_a \to qX$, we may derive the expression

$$q^2 = -\left[\frac{\vec{k}_T^2 + xm_X^2}{(1-x)}\right] + xm_a^2 \quad . \tag{16}$$

This is the square of the four vector momentum of constituent q. The constituent q (whether quark, gluon, meson,...) carries longitudinal momentum fraction x and transverse momentum $\vec{k}_T$. I have assumed that the initial hadron as well as the final hadronic system X are on-shell. While this seems to be a sensible assumption, it is by no means obvious that X is on-shell, and even if so, what mass m_X to assign to it, since X is not color neutral in the diagrams which most people draw.

If the initial constituents are assigned the off-shell spacelike four momentum required by Eq. (16), with m_X^2 treated as a positive free parameter, then the mass-singularity is removed from the physical region (unless x and $\vec{k}_T^2$ are both zero), and $d\sigma/d\vec{Q}_T^2$ no longer diverges at $\vec{Q}_T = 0$. Implementing these kinematic requirements in our $O(\alpha_s)$ computation, and integrating over the "intrinsic" $\vec{k}_T$ spectra, we would find that the theoretical curves in Fig. 11 no longer explode as $Q_T \to 0$. An excellent fit to the shape of the experimental spectra (although by no means to the absolute yield) can be achieved by proper choices of the parameters m_X^2 and $\langle \vec{k}_T^2 \rangle$. Likewise, an excellent fit can be achieved with the CIM approach.[40] Some extra care is required in dealing with off-shell initial constituents, inasmuch as the most naive procedure can lead to gauge dependence of the final answers. Proper inclusion of the off-shell effects is required in studies of large p_T processes, as well as in massive lepton pair production, especially when the hard-scattering cross-sections are convoluted with rather large intrinsic transverse momentum contributions.

Although rightfully emphasizing proper kinematic constraints, the successful fits in the small Q_T region do not address the basic question of whether the large $\vec{Q}_T$ theories are correct. For $Q_T < 1$ GeV/c, the comparison with data is being carried out in a region whether the models are inapplicable, and where the shape of the theoretical curves is controlled by parameters, such as m_X^2 and $\langle k_T^2 \rangle$, introduced by hand. In a sense the fits are dangerous in that they mislead one into thinking that more of the real small Q_T problem is solved and/or that the models are more universally applicable than is the case. The validity of the $O(\alpha_s)$ and of the CIM contributions should be judged on the behavior of the data at "large" Q_T.

Similar comments may be made regarding an entirely different method for handling data at small Q_T, proposed by Altarelli, Parisi, and Petronzio,[34] and followed by others.[41] They subtract away the infinity at $Q_T = 0$ in the simple $O(\alpha_s)$ approach and then smear this difference with an intrinsic k_T spectrum whose parameters are adjusted to fit the general shape of the experimental spectrum $d\sigma/d\vec{Q}_T^2$. A fit to the absolute normalization is enforced by requiring that the integral of the final result yield the observed integral.

5. Energy dependence

I have concentrated here so far on the description of the Q_T dependence of $d\sigma/dQ_T^2$ at fixed energy. However, as emphasized before,[3] the real test of QCD is in the energy dependence at fixed Q_T, or at fixed $Q_T/\sqrt{s}$. Indeed, insofar as Q_T dependence itself is concerned, a Gaussian fit to the data in Fig. 11 would do quite well at fixed s.

The statement of energy dependence in the $O(\alpha_s)$ QCD approach is

provided by the expression

$$\left.\frac{s^3\, d\sigma}{dQ^2\, dx_F\, dQ_T^2}\right|_{\text{large } Q_T} = f(Q^2/s\,,\, x_F\,,\, x_T) \quad , \tag{17}$$

where $x_T = 2Q_T/\sqrt{s}$. It may be contrasted with the classical scaling relation for the integrated cross-section,

$$\frac{s^2\, d\sigma}{dQ^2\, dx_F} = g(Q^2/s\,,\, x_F) \quad . \tag{18}$$

At small Q_T, where intrinsic k_T effects control the physics, the scaling relation presumably is a simple generalization of Eq. (18); vis.,

$$\left.\frac{s^2\, d\sigma}{dQ^2\, dx_F\, dQ_T^2}\right|_{\text{small } Q_T} = g(Q^2/s\,,\, x_F\,,\, Q_T^2) \quad . \tag{19}$$

All of the expectations, Eqs. (17), (18), and (19), are modified by modest logarithmic dependence on Q^2 (and Q_T^2) when the full scale-noninvariant dependences of structure functions and of α_s on Q^2 are included in the calculation. Specifically, Eq. (17) is replaced by

$$\left.\frac{s^3\, d\sigma}{dQ^2\, dx_F\, dQ_T^2}\right|_{\text{large } Q_T} = \tilde{f}(Q^2/s\,,\, x_F\,,\, x_T\,;\, \log Q^2\,,\, \log Q_T^2) \quad .$$

The contrast between Eqs. (17) and (19) is striking. No tests have been made as yet of these crucial expectations. In going from p_{lab} = 400 GeV/c at FNAL ($\sqrt{s} \simeq 27$ GeV) to $\sqrt{s} \simeq 53$ GeV at the ISR, one must double both Q_T and Q in order to keep x_T and Q^2/s fixed. Although this is admittedly a difficult task, given the luminosity limitations at the ISR, it would be valuable to verify even the expected trends over a more limited interval in Q_T.

6. Moments: mass dependence at $x_F = 0$

The use of moments of the Q_T distribution may facilitate comparisons between theory and data, in that the problematic low Q_T region can be deemphasized. For example, we may consider the quantity

$$\langle Q_T^n \, d\sigma/dQ_T^2 \rangle = \int dQ_T^2 \, \frac{Q_T^n \, d\sigma}{dQ_T^2} \quad . \tag{20}$$

For simplicity, I suppress temporarily the Q^2 and x_F dependences of $d\sigma/dQ_T^2$. Since $d\sigma/dQ_T^2$ diverges as Q_T^{-2} in the simple $O(\alpha_s)$ QCD approach, the integral in Eq. (20) converges for all $n \geq 2$. Although the integrand has no infrared or mass singularity divergence for $n \geq 2$, this does not imply that the answer is insensitive to the small Q_T region. Only for n much larger than 2 is the small Q_T region sufficiently deemphasized in the final result. Unfortunately, as n grows, so do the errors on the experimental results. As a compromise, I limit myself to $n = 2$. Dividing Eq. (20) by the full cross-section integrated over Q_T (obtained from data, or from Eq. (1) with Q^2 dependent structure functions), one may define

$$\langle Q_T^2 \rangle_{QCD} = \frac{1}{\sigma} \int Q_T^2 \, dQ_T^2 \left\{ \frac{d\sigma^{compt}}{dQ_T^2} + \frac{d\sigma^{ann}}{dQ_T^2} \right\} \quad . \tag{21}$$

This is the $O(\alpha_s)$ contribution to $\langle Q_T^2 \rangle$ if I use the first order perturbative QCD expressions for $\sigma^{compt}(qG \to q\gamma^*)$ and for $\sigma^{ann}(q\bar{q} \to \gamma^* G)$ on the right hand side. Obviously, $\langle Q_T^2 \rangle_{QCD}$ cannot be expected to reproduce $\langle Q_T^2 \rangle_{exp}$ for the same reasons that the $O(\alpha_s)$ distribution does not reproduce $d\sigma/dQ_T^2$. Thus we define

$$\langle Q_T^2 \rangle_{exp} = \langle Q_T^2 \rangle_{QCD} + \langle Q_T^2 \rangle_{correction} \tag{22}$$

where the correction term, added in quadrature, stands not only for such obvious physical effects as the neglected intrinsic transverse momentum contribution, due to confinement effects, but also covers a multitude of other errors of omission and comission.

A comparison of $\langle Q_T^2 \rangle$ with data is presented in Fig. 14. Shown is the Q^2 dependence at $y = 0$ in pN collisions at fixed energy, $p_{lab} = 400$ GeV/c. The two-body annihilation contribution has a fixed magnitude and shape, determined by the QCD cross-section and by the known quark and antiquark structure functions (Q^2 variation of these densities is ignored). The Q^2 dependence of the Compton term is somewhat less certain since the gluonic density is not as well known. To obtain the results shown, I use Eq. (14), with power $p = 6$. Choosing instead $p = 5$ (or 7), I would find a curve for the Compton contribution which rises more (or less) rapidly with Q^2 for $M > 4$ GeV. The overall normalization of the Compton contribution may also be increased if I depart from the assumption embodied in Eq. (14) and assign more than 50% of the hadron's momentum to the gluonic component. However, these uncertainties are minor. In Fig. 14, the net QCD contribution[3] to $\langle Q_T^2 \rangle$ is seen to rise with Q^2 until $M \simeq 6$ GeV, and then the flatten off near a level of ≈ 0.8 GeV^2, a factor of two or more beneath the experimental result.

Before I discuss the discrepancy in the absolute value of $\langle Q_T^2 \rangle$, it is worth noting that the shape of the Q^2 dependence of $\langle Q_T^2 \rangle_{QCD}$ is in reasonable agreement with experiment. This flat behavior of $\langle Q_T^2 \rangle_{QCD}$ vs. Q^2 for $M \gtrsim 6$ GeV may be contrasted with the naive expectation that

$$\langle Q_T^2 \rangle_{QCD} \propto Q^2 \quad . \tag{23}$$

Because QCD is not a soft field theory, one should indeed expect that at fixed $M/\sqrt{s}$ (and fixed y or x_F)

$$\langle Q_T^2 \rangle_{QCD} \propto Q^2 \, f(Q^2/s) \quad . \tag{24}$$

The flat behavior of $\langle Q_T^2 \rangle_{QCD}$ with Q^2 for $M \gtrsim 6$ GeV shows that the scaling function $f(Q^2/s)$ has a strong dependence on Q^2 at fixed s. This strong dependence is supplied by the rapidly falling antiquark and gluonic structure functions. Stated otherwise, the flat behavior of $\langle Q_T^2 \rangle_{QCD}$ with Q^2 at 400 GeV/c provides an indirect measurement of the fact that the effective power p in Eq. (14) is greater than 4 or 5.

To reach the experimental level of $\langle Q_T^2 \rangle \simeq 1.8$ GeV^2 in Fig. 14, one must add ≈ 1 GeV^2 to the $O(\alpha_s)$ QCD result. Part of this supplement is surely associated with the non-perturbative, intrinsic $\langle k_T^2 \rangle$ carried by each constituent, due to the constituent's confinement in a hadron of limited transverse size. In their global fit to $d\sigma/dQ_T^2$, Altarelli, Parisi, and Petronzio[34] also found that their "intrinsic" component has $\langle k_T^2 \rangle \approx 1$ GeV^2.

If we divide 1 GeV^2 equally between each of the two initial constituents, we find that we are asking that confinement supply a rather hefty $\langle k_T^2 \rangle \approx 0.5$ GeV^2, or $\langle k_T \rangle = 600$ MeV, instead of the more typical 300 MeV. A similarly large number is invoked in some aspects of fits[42] to data on correlations at large p_T; ρ mesons[43] as well as hadronic clusters are observed to be produced with $\langle p_T \rangle \approx 600$ MeV. Nevertheless, $\langle k_T \rangle \approx 600$ MeV is uncomfortably large for several reasons. First, it raises the technical issue of our neglect of off-shell kinematics. Returning to Eq. (16), we see that if our fit requires $\langle k_T^2 \rangle \approx 0.5$ GeV^2,

we are treading close to inconsistency in ignoring the off-shell nature of the initial constituents. Second, there is a more important issue of principle to be faced. In evaluating the $O(\alpha_s)$ QCD terms, we pretend to have identified the essential hard scattering, large Q_T effects. However, in the end, we must hide more than half of the observed $\langle Q_T^2 \rangle$ in an uncalculated contribution. All of the large Q_T is not "out in the open", as it should be.

I know of no explicit calculation of $\langle Q_T^2 \rangle_{QCD}$ in the DDT approach,[23] but it seems clear that the residual unexplained portion of $\langle Q_T^2 \rangle$ will be decreased if the DDT method is implemented. This effect is correlated with the fact that the cross-section $d\sigma/dQ_T^2$ in the DDT approach flattens as Q_T decreases. In the DDT approach, one may well achieve values of the intrinsic $\langle k_T \rangle$ closer to the expected 300 MeV.

In the CIM approach, it should be mentioned that Duong-van and Blankenbecler[18] calculated values of $\langle Q_T^2 \rangle \simeq 1.8$ GeV^2 and $\langle Q_T \rangle \simeq 1.2$ GeV, which later data fully supported. In obtaining their results, they used full off-shell kinematics. Thus, the large Q_T CIM effects and the "intrinsic" contributions are combined directly in their answer.

7. Moments: x_F and quantum number dependences

In the previous paragraphs I discussed the behavior of $\langle Q_T^2 \rangle_{QCD}$ as a function of Q^2 at fixed x_F, concentrating on pN collisions at 400 GeV/c for comparisons with data. Data are available also on the x_F and s dependences of $\langle Q_T^2 \rangle$ in pN collisions,[4,5] and on the Q^2 and x_F dependences in π^-N collisions[9] at 225 GeV/c.

The π^-N data allow us to examine a situation in which the valence-valence process is dominant. At large Q_T, the two-body annihilation

reaction $q\bar{q} \to \gamma^* G$ should dominate the Compton process $qG \to \gamma^* q$. For the $\pi^- N$ calculations, I used a gluon density in the pion suggested by constituent counting rules,[30] again normalized to 50% of the pion's momentum:

$$xG_\pi(x) = 2(1-x)^3 \quad . \tag{25}$$

At the time I did the calculations reported here, the quark structure function of the pion had not been determined. Thus, I tried a few different forms for $xq_\pi(x)$, to see what differences arise in the final results. Shown in Fig. 15 are values of $\langle Q_T^2 \rangle_{QCD}$ which I obtained from my $O(\alpha_s)$ calculations, for three choices of the quark structure function of the pion. As before, I employ massless and on-shell initial and final elementary constituents in the computations. The three choices are: (a) "FF", the pion structure function suggested in Ref. 44, for which $xq_\pi(x) \to (1-x)^0$ as $x \to 1$; (b) "Dao et al.", from Ref. 45, for which $xq_\pi(x) \to (1-x)^{2.55}$ as $x \to 1$; and (c) a purely ad-hoc form whose explicit structure is

$$xq_v(x) = 0.35\ (1-x)^{0.6} \tag{26}$$

$$xq_\pi(x) = xq_v(x) + 0.1\ (1-x)^5 \quad . \tag{27}$$

All three "models" in Fig. 15 yield essentially identical results for $x_F < 0$, in the target nucleon's "fragmentation region". For $x_F > 0$, differences are marked, both in normalization and x_F dependence, due to the different behavior of the three pion structure functions. Nevertheless, all three models fail to reproduce the size of $\langle Q_T^2 \rangle_{exp}$, which is again roughly a factor of two above the calculations at 225 GeV/c.

In order to compare results with πN data on $\langle Q_T \rangle$, I again add a "confinement" contribution in quadrature to the QCD $O(\alpha_s)$ result, using

the same value $\langle Q_T^2 \rangle_{conf} = 1.04\ GeV^2$, determined in the fit to pN collisions at 400 GeV/c and y = 0. To limit arbitrary freedom, I assume that the value 1.04 GeV^2 is independent of Q^2, s, and x_F, and of quantum number effects. To obtain a value of $\langle Q_T \rangle$ from the resulting $\langle Q_T^2 \rangle$, one must assume a form for the distribution $d\sigma/dQ_T^2$, which I take to be the form fitted to the pN data.[4] Thus,

$$\langle Q_T \rangle = 0.859 \langle Q_T^2 \rangle^{\frac{1}{2}} \quad . \tag{28}$$

A comparison of the calculated values of $\langle Q_T \rangle$ with data on the Q^2 dependence at $x_F = 0.2$ is shown in Fig. 16, and with data on the x_F dependence in Fig. 17. The models with relatively flat quark structure functions are capable of reproducing both the magnitude and general shape of $\langle Q_T \rangle$ as a function of both x_F and Q^2. Judging from the fact that the results obtained with the $(1-x)^{0.6}$ form pass systematically through the lower portion of the error flags in Figs. 16 and 17, I imagine that calculations based on the "true" spin-averaged structure function $\propto (1-x)^1$, will do somewhat worse. However, here again, a proper calculation should be done including a full treatment of spin effects.[13] The agreement of these "predictions" with the data is satisfactory.

It is interesting to observe that

(i) $\langle Q_T \rangle^{\pi N}_{225\ GeV/c} \approx \langle Q_T \rangle^{pN}_{400\ GeV/c}$; (Data)

(ii) $\langle Q_T^2 \rangle^{\pi N,\ 225\ GeV/c}_{QCD} \approx \langle Q_T^2 \rangle^{pN,\ 400\ GeV/c}_{QCD}$; (Theory)

This suggests that the discrepancy between $\langle Q_T^2 \rangle_{QCD}$ and experiment, from whatever origin, is roughly universal. Valence-valence processes are not endowed with a much larger or a much smaller "intrinsic" portion of $\langle Q_T^2 \rangle$ than the valence-ocean pN reaction.

The comparisons with the data in Figs. 16 and 17 suggest that improved agreement would be obtained if the "intrinsic" $\langle k_T^2 \rangle$ contribution is modestly larger in pions than in nucleons, and if the intrinsic $\langle k_T^2 \rangle$ grows with x. More explicitly, if we imagine a quark structure function $q(x,k_T^2)$, it should be true that $\langle k_T^2(x) \rangle_\pi$ grows slowly with x, and that $\langle k_T^2(x) \rangle_\pi > \langle k_T^2(x) \rangle_N$. Although little on the x_F dependence of $\langle Q_T \rangle$ is available from pN collisions, the results[4,5] show a rather flat behavior of $\langle Q_T^2 \rangle$ vs. x_F, in disagreement with the results of my $O(\alpha_s)$ calculation in Fig. 18. This comparison suggests again that the intrinsic $\langle k_T^2(x) \rangle_N$ should grow with x.

In an interesting paper based largely on simple kinematic arguments, Ellwanger shows that $\langle k_T^2(x) \rangle$ is determined by the x dependence of the structure functions.[46] In particular, he derives

$$\langle k_T^2(x) \rangle = \frac{x(1-x)}{xq(x)} \int_x^1 \left(\frac{m_X^2}{(1-x')^2} - m_a^2 \right) q(x')\, dx' \quad . \qquad (29)$$

Here m_X is the mass of the (on-shell) system X which results from the hadronic dissociation $h_a \to qX$, and m_a is the mass of the incident hadron h_a. This equation would yield an absolute determination of $\langle k_T^2(x) \rangle$ except for uncertainties associated with m_X^2 (which itself may be a function of x). Taking m_X^2 to be constant, Ellwanger obtains curves of $\langle k_T^2(x) \rangle$ which grow with x. Choosing $xq(x) \propto (1-x)^3$, appropriate for nucleons, and $m_X = 1$ GeV, he finds that $\langle k_T^2(x) \rangle_{valence}$ changes from about 0.25 GeV^2 at $x = 0.2$ to 0.45 GeV^2 at $x = 0.8$. Ellwanger shows that as $x \to 1$,

$$\langle k_T^2(x) \rangle \to m_X^2 / (n-1) \quad , \qquad (30)$$

where n is the power in an expansion of $xq(x) \propto (1-x)^n$, valid near $x = 1$. Therefore, although $\langle k_T^2(x)\rangle_{sea}$ also grows with x, it is smaller at a given x than $\langle k_T^2(x)\rangle_{valence}$. Whereas the desired growth of the intrinsic contribution with x is obtained, the size of $\langle k_T^2(x)\rangle_{valence} + \langle k_T^2(x)\rangle_{sea}$ cannot be made as large as the required 1 GeV^2 unless $m_X^2 \simeq 3$ GeV^2, which is perhaps too large. This is another argument against attributing all of the discrepancy between $\langle Q_T^2\rangle_{exp}$ and $\langle Q_T^2\rangle_{QCD}$ to intrinsic transverse momentum effects. Note, finally, that Eq. (30) implies that

$$\langle k_T^2(x)\rangle_\pi > \langle k_T^2(x)\rangle_N \quad , \tag{31}$$

unless the value of m_X^2 is much smaller in π dissociation than in N dissociation.

8. Energy dependence of $\langle Q_T^2\rangle$

On purely dimensional grounds we may argue that $\langle Q_T^2\rangle_{QCD} \propto sg(Q^2/s, x_F)$ for large Q^2. Assuming that the non-QCD "intrinsic" portion of $\langle Q_T^2\rangle$ is independent of s at fixed Q^2/s and x_F, as seems reasonable, we deduce that

$$\langle Q_T^2\rangle = a(Q^2/s\,,\, x_F) + sb(Q^2/s\,,\, x_F) \quad . \tag{32}$$

Allowing for scaling violtions, the function $b(Q^2/s) \to b(Q^2/s) / \log Q^2$. If there is some cross-talk between the QCD and "intrinsic" contributions, a term $\propto \sqrt{s}$ may also be present on the right hand side of Eq. (32).

To first order in α_s, the function $b(Q^2/s, x_F)$ in Eq. (32) may be obtained directly from a computation of the graphs in Fig. 10. Results are shown in Fig. 19; they may be used for predicting values of $\langle Q_T^2\rangle$ at various energies. For example, at $M/\sqrt{s} = 0.1$, I calculate $b = 0.73 \times 10^{-3}$ GeV^{-2}, implying that at $M/\sqrt{s} = 0.1$ and $\sqrt{s} = 62$ GeV, $\langle Q_T^2\rangle = 1.0 + 2.8 =$

3.8 GeV^2. This expectation agrees well with the measurement of $\langle Q_T^2 \rangle_{exp} = 4.2 \pm 0.9$ GeV^2 reported by the CERN-Columbia-Oxford-Rockefeller ISR collaboration.[6] A comparison of the predicted energy dependence with Fermilab data[4] is shown in Fig. 20.

The energy dependence of $\langle Q_T^2 \rangle$ expected from QCD arguments is certainly consistent with experiment. In the CIM approach,[18] $\langle Q_T^2 \rangle$ is expected to rise slightly in the Fermilab range, and to tend to a constant as $s \to \infty$. The ISR results rule out CIM as the full answer, but, as remarked earlier, present data on $d\sigma/dQ_T^2$ in the intermediate Q_T range appear to require the CIM terms.

As discussed in Section V.5, convincing tests of QCD must be carried out at "large Q_T", where reasonably reliable predictions are available for the energy, x_F, and Q_T dependences of $d\sigma/dQ_T^2$, including absolute normalization, and systematics associated with the quantum numbers of the incident beams.[3] Moments of the Q_T distribution tend to be unreliable guides since a great deal of the integral comes from the low Q_T region where use of the theory is inappropriate.

VI. Conclusions and Outlook

The ever improving quality of high-energy data[4-11] on massive lepton pair production now permits reasonably detailed tests of several theoretical ideas. More progress may be expected within the coming year or so as new results emerge from experiments at Fermilab and at CERN. In pN collisions, exploration of a broad range in $x_F = x_p - x_N$ will complement the excellent data now confined largely to $x_F = 0$ and make possible a thorough investigation of the (valence) quark structure function of the

nucleon in the timelike ($Q^2 > 0$) region, especially for large x_p ($x_p > 0.5$). In both pN and πN reactions, we can look forward to accurate measurements of the full angular distribution $W(\theta^*,\phi^*)$ in the lepton pair rest frame, including variations with x_F and Q_T. These distributions should yield some insight into bound state mechanisms,[13] and, at large enough $\vec{Q}_T$, test features of perturbative QCD.[47] Visionaries may seek signals in $W(\theta^*,\phi^*)$ associated with weak-electromagnetic interference (γ^*,Z^o). Extending the range of measurements of $d\sigma/d^2\vec{Q}_T$ to higher $\vec{Q}_T$ poses experimental challenges, but seems necessary for clean tests of the ideas reviewed in Section V. Better data on the Q^2 and s dependences of cross-sections may permit the identification of scaling violations expected theoretically in $d\sigma/dQ^2dx_F$ and in $d\sigma/dQ^2\,dx_F\,d^2\vec{Q}_T$.

Little information exists now on the properties of the hadronic spray which accompanies a massive lepton pair. At large $\vec{Q}_T$, the virtual photon should be balanced by a quark jet in pN collisions and by a gluon jet in π^-N and $\bar{p}$N reactions. It would be useful to design experiments to investigate these companion systems. In addition, two roughly longitudinal jets of hadrons should be present in each event, one the debris of the projectile, and the other of the target. The charge and momentum distributions in these longitudinal jets are expected to yield further insight into hadronic structure.[48]

The proven viability of the Drell-Yan process as a probe of hadronic structure should encourage future high-energy studies with antiproton beams and with polarized nucleon beams and targets.

On the theoretical side, the necessity for QCD, or for some similar theoretical scheme, seems evident for at least two reasons: scaling

violations, and the observed large values of $\langle Q_T \rangle$. However, in both deep inelastic scattering and massive lepton pair production, much has to be done yet to identify and separate the logarithmic scaling violations associated with asymptotic freedom from the perhaps more mundane scaling violations of an inverse power nature ($\propto Q^{-2}$), expected on general physical grounds.[49] Detailed work is desirable, leading to quantitative estimates of the magnitude of the Q^{-2} terms and of their functional dependence on various kinematic variables such as x_F and $\vec{Q}_T$. In the realm of logarithmic, log Q^2 QCD effects, there is already evidence in both deep inelastic processes[20] and in massive lepton pair production that one must go beyond the leading logarithm approximation in computing observables for comparisons with data. The next to leading, non-factorizing $1/\log Q^2$ correction terms in lepton pair production may be as large as the leading terms (cf., Section IV.2) in the range of Q^2 now being explored ($20 \lesssim Q^2 \lesssim 100$ GeV^2). If so, a new method must be devised to reorder the perturbation series in log Q^2.

Techniques are also being developed[36,38] for handling the domain in which both Q^2 and Q_T^2 are large, but more work along these lines is needed, as well as on the problem of continuing the results to small Q_T^2. Finally, it would be highly desirable to go beyond the stage of elementary constituent scattering cross sections and of probabilistic formulas such as Eqs. (1) and (3), and to deal more directly with the fact that the incident and final hadronic states are bound systems.

ACKNOWLEDGEMENTS

In preparing this report, I have benefitted greatly from discussions with many colleagues at SLAC.

REFERENCES

1. S. D. Drell and T. M. Yan, Phys. Rev. Lett. 25, 316 (1970), 25, 902 (1970), and Ann. Phys. (N.Y.) 66, 578 (1971). For a recent general discussion, see C. S. Lam and Wu-Ki Tung, Phys. Rev. D18, 2447 (1978).

2. For a recent review of the data, see L. Lederman, Proceedings of the 19th International Conference on High Energy Physics, Tokyo, 1978. Edited by S. Homma, M. Kawaguchi and H. Miyazawa.

3. E. L. Berger, Proceedings of the 1978 Vanderbilt Conference, AIP Conference Proceedings Series, No. 45, Edited by R. S. Panvini and S. E. Csorna; and in Hadron Physics at High Energies, 1978 Marseille (France) Workshop, Edited by C. Bourrely, J. Dash and J. Soffer.

4. Columbia-Fermilab-Stony Brook Collaboration (FNAL), J. K. Yoh et al., Phys. Rev. Lett. 41, 684 (1978) and 41, 1083 (1978), plus references cited therein, as well as Ref. 2.

5. Seattle-Northeastern-Michigan-Tufts Collaboration (FNAL), S. Childress et al., Report No. NUB-2370, submitted to the Tokyo Conference, 1978.

6. CERN-Columbia-Oxford - Rockefeller Collaboration (ISR), A. L. S. Angelis et al., Report No. COO-2232A-69, September 1978, submitted to the Tokyo Conference, 1978.

7. CERN-Harvard-Frascati-MIT-Naples-Pisa Collaboration (ISR), F. Vannucci, contribution to the Karlsruhe Summer Institute, 1978.

8. Athens-Brookhaven-CERN-Syracuse-Yale Collaboration (ISR), C. Kourkoumelis et al., Brookhaven Report BNL-25075 (1978) and references cited therein, plus I. Mannelli, Tokyo Conference report.

9. Chicago-Illinois-Princeton Collaboration (FNAL), C. B. Newman et al., Phys. Rev. Lett. 42, 951 (1979); G. E. Hogan et al., Phys. Rev. Lett. 42, 948 (1979); and K. J. Anderson et al., Phys. Rev. Lett. 42, 944 (1979).

10. Birmingham-CERN-Munich-Neuchatel-Ecole Polytechnique-Rutherford Collaboration (CERN-SPS), M. J. Corden et al., Phys. Lett. 76B, 226 (1978). See also J. Alspector et al., Phys. Lett. 81B, 397 (1979).

11. Saclay-Imperial College-Southampton-Indiana Collaboration (CERN-SPS), M. A. Abolins et al., Saclay report DPhPE 78-05 (August 1978), paper submitted to the Tokyo Conference, 1978.

12. For reviews of dynamics at large p_T, see M. Jacob and P. Landshoff, Phys. Reports 48, 285 (1978); S. J. Brodsky, SLAC-PUB-2298, Lectures presented at the La Jolla Summer Workshop on QCD, 1978, and SLAC-PUB-2217, invited talk presented at the Symposium on Jets in High Energy Collisions, Copenhagen, 1978; R. D. Field, Jr., Tokyo, 1978 (op. cit.); and S. D. Ellis and R. Stroynowski, Rev. Mod. Phys. 49, 753 (1977).

13. E. L. Berger and S. J. Brodsky, Phys. Rev. Lett. 42, 940 (1979).

14. CERN-Dortmund-Heidelberg-Saclay Collaboration (CERN-SPS), J. G. H. deGroot et al., CERN Report November 1978, submitted to Zeitschrift fur Physik.

15. Aachen-Bonn-CERN-London-Oxford-Saclay Collaboration, P. C. Bosetti et al., Nucl. Phys. B149, 13 (1979) and B142, 1 (1978).

16. Harvard-Chicago-Illinois-Oxford Collaboration, W. A. Loomis et al., Fermilab Report 78/94-Exp. (1978), and H. L. Anderson et al., Phys. Rev. Lett. 40, 1061 (1978).

17. M. D. Mestayer, SLAC Report No. 214 (1978) and references therein.

18. M. Duong-van, K. V. Vasavada and R. Blankenbecler, Phys. Rev. D16, 1389 (1977); M. Duong-van and R. Blankenbecler, Phys. Rev. D17, 1826 (1978).

19. See, for example, L. Abbott, SLAC-PUB-2296 (1979), to be published in the Proceedings of the 1979 Coral Gables Conference, Orbis Scientiae, 1979; I. Schmidt and R. Blankenbecler, Phys. Rev. D16, 1318 (1977); and H. Harari, SLAC-PUB-2254 (1979), submitted to Nucl. Phys.

20. For an excellent review of the uses of QCD in deep inelastic scattering, including higher order corrections, see A. J. Buras, Fermilab report 79/17-THY (1979). See also G. C. Fox, Caltech Report 68-658 (1978), Invited review presented at the Purdue Conference on Neutrino Physics, Lafayette, Indiana.

21. H. D. Politzer, Phys. Lett. 70B, 430 (1977), and Nucl. Phys. B129, 301 (1977); C. T. Sachrajda, Phys. Lett. 73B, 185 (1977); H. Georgi, Phys. Rev. D17, 3010 (1978); G. Altarelli, G. Parisi and R. Petronzio, Phys. Lett. 76B, 351 (1978); J. Frenkel, M. J. Shailer and J. C. Taylor, Nucl. Phys. B148, 228 (1979).

22. R. K. Ellis et al., Phys. Lett. 78B, 281 (1978); C. H. Llewellyn Smith, Schladming Lectures, Oxford Report 47/78 (1978); D. Amati, R. Petronzio and G. Veneziano, Nucl. Phys. B140, 54 (1978), and B146, 29 (1978); S. Gupta and A. H. Mueller, Columbia Report CU-TP-139 (1979); S. B. Libby and G. Sterman, Phys. Rev. D18, 3252 (1978); R. C. Hwa and J. Wosiek, Rutherford Report RL-78-82 (1978).

23. Y. L. Dokshitser, D. I. D'Yakonov and S. I. Troyan, "Inelastic Processes in Quantum Chromodynamics," from the XIIIth Winter School of Leningrad B. P. Konstantinov Institute of Nuclear Physics (1978), SLAC Translation No. 183.

24. G. Altarelli, R. K. Ellis and G. Martinelli, MIT Report CTP No. 776 (1979); J. Kubar-Andre and F. E. Paige, Phys. Rev. D19, 221 (1979); K. Harada, T. Kaneko and N. Sakai, CERN Report TH-2619 (1979); J. Abad and B. Humpert, Phys. Lett. 80B, 286 (1979), and Wisconsin Report COO-881-57 (1978); J. Kripfganz and A. P. Contogouris, McGill Report 79-0049 (1979).

25. See, e.g., S. J. Brodsky and G. P. Lepage, SLAC-PUB-2294 (1979) and references therein.

26. C. T. Sachrajda and R. Blankenbecler, Phys. Rev. D12, 3624 (1975).

27. T. Goldman, M. Duong-van and R. Blankenbecler, SLAC-PUB-2283 (1979).

28. C. E. DeTar, S. D. Ellis and P. V. Landshoff, Nucl. Phys. B87, 176 (1975).

29. J. Ellis, M. K. Gaillard and W. J. Zakrezewski, Phys. Lett. 81B, 224 (1979); R. D. Carlitz and D. B. Creamer, University of Pittsburgh, Report No. PITT-208 (1978).

30. S. J. Brodsky and G. Farrar, Phys. Rev. Lett. 31, 1153 (1973); V. Matveev et al., Lett. Nuovo Cimento 7, 719 (1973); F. Ravndal, Phys. Lett. 47B, 67 (1973); A. Vainshtein and V. Zacharov, Phys. Lett. 72B, 368 (1978); R. Blankenbecler and S. J. Brodsky, Phys. Rev. D10, 2973 (1974).

31. S. D. Drell, D. J. Levy and T. M. Yan, Phys. Rev. D1, 1617 (1970); G. Farrar and D. Jackson, Phys. Rev. Lett. 35, 1416 (1975).

32. For estimates of the effects of scaling violations on $d\sigma/dQ^2dy$, see R. D. Field, Ref. 12.

33. M. Holder et al., Phys. Lett. 69B, 377 (1977).

34. G. Altarelli, G. Parisi and R. Petronzio, Phys. Lett. 76B, 351 (1978); Phys. Lett. 76B, 356 (1978); R. Petronzio, CERN Report TH-2495 (1978).

35. H. Fritzsch and P. Minkowski, Phys. Lett. 73B, 80 (1978); C. Michael and T. Weiler, contribution to the XIIIth Rencontre de Moriond, Les Arcs, France (1978); K. Kajantie and R. Raitio, Nucl. Phys. B139, 72 (1978); K. Kajantie, J. Lindfors and R. Raitio, Nucl. Phys. B144, 422 (1978); F. Halzen and D. Scott, Phys. Rev. D19, 216 (1979), D18, 3378 (1978), and Phys. Rev. Lett. 40, 1117 (1978); K. Kinoshita and Y. Kinoshita, Prog. Theor. Phys. 61, 526 (1979); M. Gluck and E. Reya, Nucl. Phys. B145, 24 (1978); H. Georgi, Phys. Rev. Lett. 42, 294 (1978).

36. Yu. L. Dokshitzer, D. I. Dyakonov and S. I. Troyan, Phys. Lett. 78B, 290 (1978).

37. K. Kajantie and J. Lindfors, Nucl. Phys. B146, 465 (1978).

38. G. Parisi and R. Petronzio, CERN Report Ref. TH-2627 (1979).

39. R. Blankenbecler, S. J. Brodsky and J. F. Gunion, Phys. Rev. D6, 2652 (1972).

40. C. Debeau and D. Silverman, Phys. Rev. D18, 2435 (1978), and SLAC-PUB-2187 (1978).

41. See some of the papers listed in Ref. 35.

42. R. P. Feynman, R. D. Field and G. C. Fox, Phys. Rev. D18, 3320 (1978), and Nucl. Phys. B128, 1 (1977).

43. British-French-Scandinavian Collaboration, M. G. Albrow et al., CERN Report, December 1978, submitted to Nucl. Phys.

44. R. D. Field and R. P. Feynman, Phys. Rev. D15, 2590 (1977).

45. F. T. Dao et al., Phys. Rev. Lett. 39, 1388 (1977).

46. U. Ellwanger, Heidelberg Report HD-THEP-78-19 (1978).

47. See, e.g., R. Thews, Arizona Report, January 1979; K. Kajantie, J. Lindfors and R. Raitio, Phys. Lett. 74B, 384 (1978); E. L. Berger, J. Donohue and S. Wolfram, Phys. Rev. D17, 858 (1978).

48. See, e.g., T. A. DeGrand, SLAC Report: SLAC-PUB-2182 (August 1978); and T. A. DeGrand and H. I. Miettinen, Phys. Rev. Lett. 40, 612 (1978).

49. See, e.g., I. Schmidt and R. Blankenbecler, Ref. 19; and E. L. Berger and S. J. Brodsky, Ref. 13.

FIGURE CAPTIONS

1. Basic Drell-Yan quark-antiquark annihilation mechanism for lepton pair production in hadronic collisions, illustrated here for $h_a h_b \to \mu\bar{\mu}X$; q and $\bar{q}$ denote respectively a quark and an antiquark constituent.

2. The energy dependence of $\langle Q_T \rangle$ for $pN \to \ell\bar{\ell}X$. Shown are Fermilab data at $p_{lab} = 200$, 300, and 400 GeV/c [Ref. 4] and an ISR point at $\sqrt{s} = 62$ GeV [Refs. 6 and 8]. All data are at rapidity $y \approx 0$. For the FNAL points $0.2 < M/\sqrt{s} < 0.5$, whereas for the ISR point $M/\sqrt{s} \approx 0.1$. The ISR point is an average of the values of 1.67 ± 0.21 GeV for $6.0 < M < 8.75$ GeV quoted by the CCOR group (Ref. 6), and 2.1 ± 0.6 GeV for $6 < M < 7$ GeV quoted by the ABCSY group (Ref. 7). The straight line fit shown is only one of many phenomenological forms which would interpolate between the FNAL and ISR data.

3. Series of diagrams illustrating the interactions of free quark, antiquark, and gluon constituents: (a) the basic zero order Drell-Yan process $q\bar{q} \to \gamma^*$; (b) and (c) the first order $O(\alpha_s)$ Compton processes $qG \to \gamma^* q$; (d) and (e) the first order two body annihilation process $q\bar{q} \to \gamma^* G$; (f),(g) and (h), a sample of second order, $O(\alpha_s^2)$, processes. Not drawn are many other diagrams in $O(\alpha_s^2)$ related by gauge invariance requirements to those shown.

4. Diagrams for $Mq \to q\gamma^*$, $\gamma^* \to \mu\bar{\mu}$. Here M denotes a meson. Solid lines represent quarks. Symbols p_1, p_a, p_b and p_c denote four-momenta of quarks, and k is the four-momentum of the gluon. Both (a) and (b) are required by gauge invariance, although in a physical (axial) gauge, the scaling contributions as $Q^2 \to \infty$ can be identified solely with (a).

5. A diagram illustrating an initial state interaction (Pomeron exchange (?)), as well as the final-state evolution of the "spectator" quarks, from hadrons h_a and h_b, into observed color-singlet hadrons.

6. The spin averaged structure function $f^{\pi^-}(x) = x\bar{u}_\pi(x)$ obtained by the Chicago-Princeton collaboration, Ref. 9. The solid line is a fit to the form $a\sqrt{x}(1-x)^b$ with $a = 0.90 \pm 0.06$ and $b = 1.27 \pm 0.06$.

7. A test of the classical scaling prediction with data on $pN \to \mu\bar{\mu}X$ at 200, 300, and 400 GeV/c, by the Columbia-Fermilab-Stony Brook collaboration [Ref. 4]. The data are centered at rapidity $y = 0.2$ at each energy. In part (a), the scaling quantity $sd^2\sigma/dyd\sqrt{\tau}$ is shown; $\tau = Q^2/s$. A simple function $F(\tau)$ is fitted to these data points. The results in (b) are obtained by dividing those in (a) by $F(\tau)$; the scatter of points illustrates the deviations from perfect scaling.

8. Comparison of FNAL data (CFS, Ref. 4) on $pN \to \mu\bar{\mu}X$ with CERN-ISR data on $pp \to \mu\bar{\mu}X$ (CHFMNP, Ref. 7) and $pp \to e^+e^-X$ (ABCSY, Ref. 8) in terms of the scaling quantity $M^3d\sigma/dM$. Note that these data are integrated over $x_F > 0$; the figure is adapted from Ref. 7. The Υ region in the FNAL data ($\sqrt{\tau} \simeq 0.35$) is omitted.

9. A comparison of the sea distribution obtained from $pN \to \mu\bar{\mu}X$, via the classical Drell-Yan formula, with that determined in deep-inelastic neutrino scattering. The neutrino points are extracted from Ref. 14.

10. The first order, $O(\alpha_s)$, QCD contributions to $h_1h_2 \to \gamma X$ at large Q_T. Shown are the "Compton" set $Gq \to \gamma q$ and the two body annihilation set $\bar{q}q \to G\gamma$.

11. Data from Ref. 4 are shown on the Q_T distribution of $pN \to \mu\bar{\mu}X$ at 400 GeV/c and $y = 0$ in the dimuon mass interval $7 \leq M \leq 8$ GeV. Shown also are calculations of the $O(\alpha_s)$ QCD expectations for this distribution, from Ref. 3. The solid curve marked "total" is obtained from an incoherent addition of the Compton and annihilation contributions. Indicated by cross-hatching is the critical $Q_T \approx$ 1 GeV below which the perturbation calculation is inapplicable. The comparison of theory and experiment is similar for other values of M (not shown).

12. (a) The CIM diagrams for the process $Mq \to \gamma^* q$;
(b) CIM diagrams for $Mq \to \pi q$.

13. A comparison of the CIM and QCD $O(\alpha_s)$ contributions to the muon pair cross-section $d\sigma/dM\,dy\,dQ_T^2$ for $pN \to \mu\bar{\mu}X$ at $\sqrt{s} = 27.4$ GeV, $y = 0$, and $M = 5.5$ GeV. This figure is taken from Ref. 40. The mass-singularity divergences at $Q_T = 0$ have been removed through the use of off-shell kinematics for initial and final constituents.

14. Shown are values of $\langle Q_T^2 \rangle$. The short dashed line illustrates the value obtained from the annihilation process $q\bar{q} \to G\mu\bar{\mu}$, and the dot-dashed line represents the contribution of the Compton process $qG \to q\mu\bar{\mu}$. The dotted line is the net QCD contribution to $\langle Q_T^2 \rangle$ to first order in α_s; it is obtained by addition of the Compton and annihilation portions. The solid line is obtained from the "net QCD" curve by addition of the constant "confinement" contribution 1.04 GeV^2. The data are from Ref. 4. All curves are calculated for the process $pN \to \ell^+\ell^- X$ at $p_{lab} = 400$ GeV/c and $y = 0$.

15. The $O(\alpha_s)$ QCD results for $\langle Q_T^2 \rangle$ are shown as a function of x_F for $\pi^- N \to \mu\bar{\mu}X$ at 225 GeV/c and $M_{\mu\bar{\mu}} = 7$ GeV. Values are presented for three choices of the quark structure function of the pion.

16. For $\pi^- N \to \mu\bar{\mu}X$ at $p_{lab} = 225$ GeV/c, calculated values of $\langle Q_T \rangle$ are compared with data as a function of muon pair mass, at $x_F = 0.2$; results are shown for two choices of the quark structure function of the pion.

17. For $\pi^- N \to \mu\bar{\mu}X$ at $p_{lab} = 225$ GeV/c, QCD expectations for $\langle Q_T \rangle$ are compared with data as a function of x_F at $M_{\mu\bar{\mu}} = 7$ GeV; theoretical results are shown for three choices of the quark structure function of the pion.

18. A prediction for the dependence of $\langle Q_T^2 \rangle_{QCD}$ on the longitudinal momentum fraction x_F of the lepton pair in pN collisions at 400 GeV, at the lepton pair mass M = 5 GeV.

19. In the expression $\langle Q_T^2 \rangle = a + bs$, the slope b computed from the first order QCD graphs is shown as a function of $M/\sqrt{s}$. These slopes can be used to obtain predictions for $\langle Q_T^2 \rangle$ at various lab energies and lepton pair masses.

20. Shown are the $O(\alpha_s)$ QCD expectations for the mean transverse momentum $\langle Q_T \rangle$ of lepton pairs produced in $pN \to \mu\bar{\mu}X$ at $y = 0$ and $p_{lab} = 200$ and 400 GeV/c, compared with CFS data (Ref. 4). Details of the theoretical calculation may be found in Ref. 3.

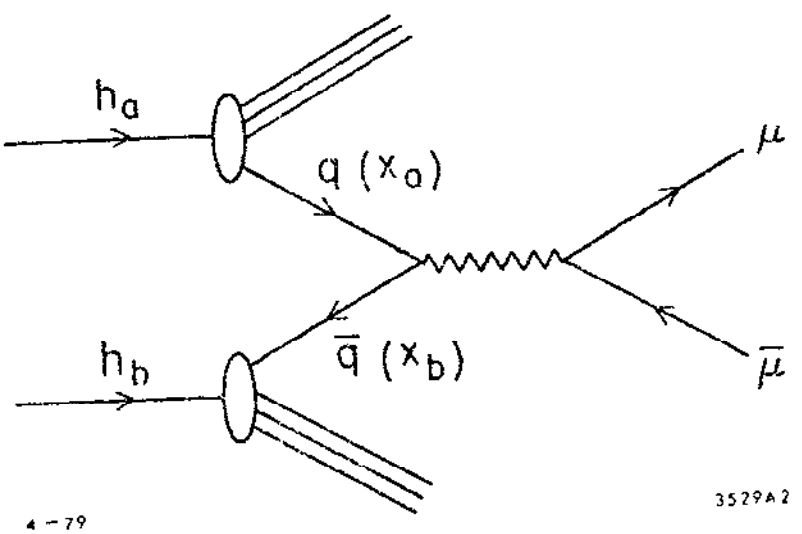

Fig. 1

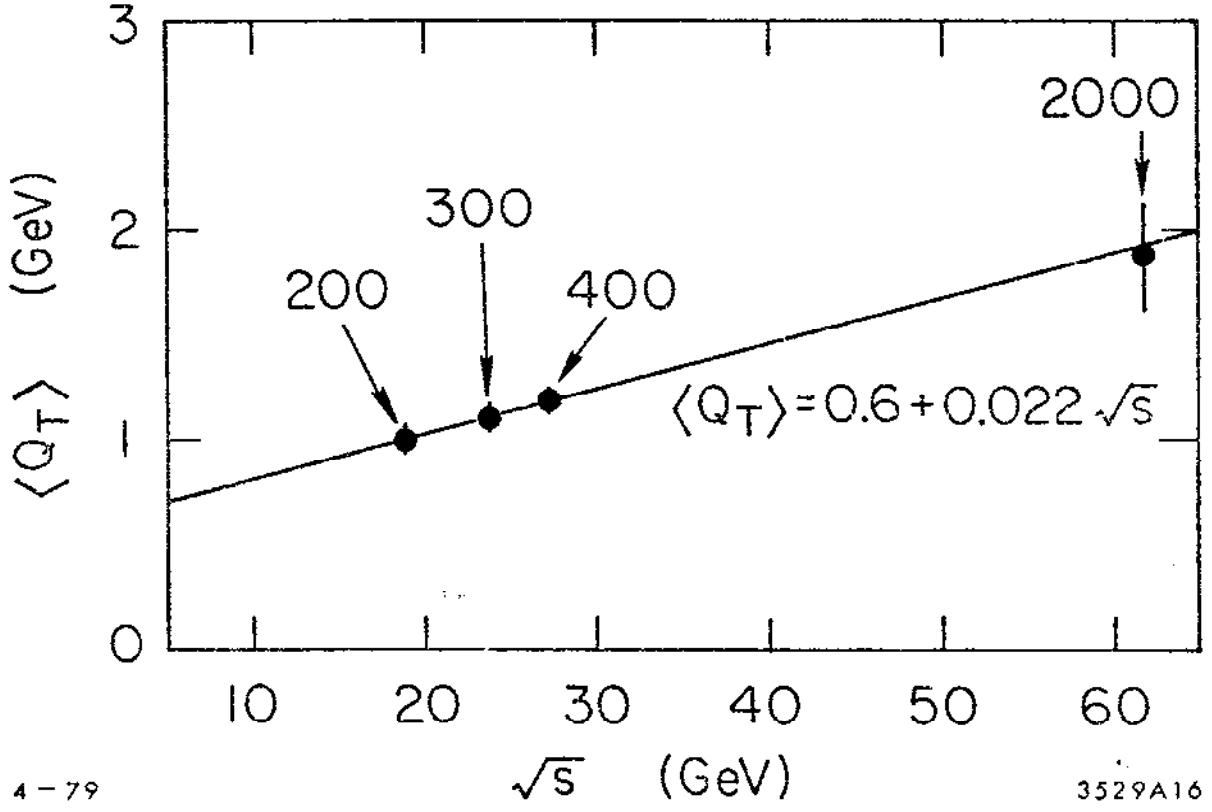
3
2
1
0
$\langle Q_T \rangle$ (GeV)
2000
300
200
400
$\langle Q_T \rangle = 0.6 + 0.022\sqrt{s}$
10
20
30
40
50
60
$\sqrt{s}$ (GeV)
4 – 79
3529A16

Fig. 2

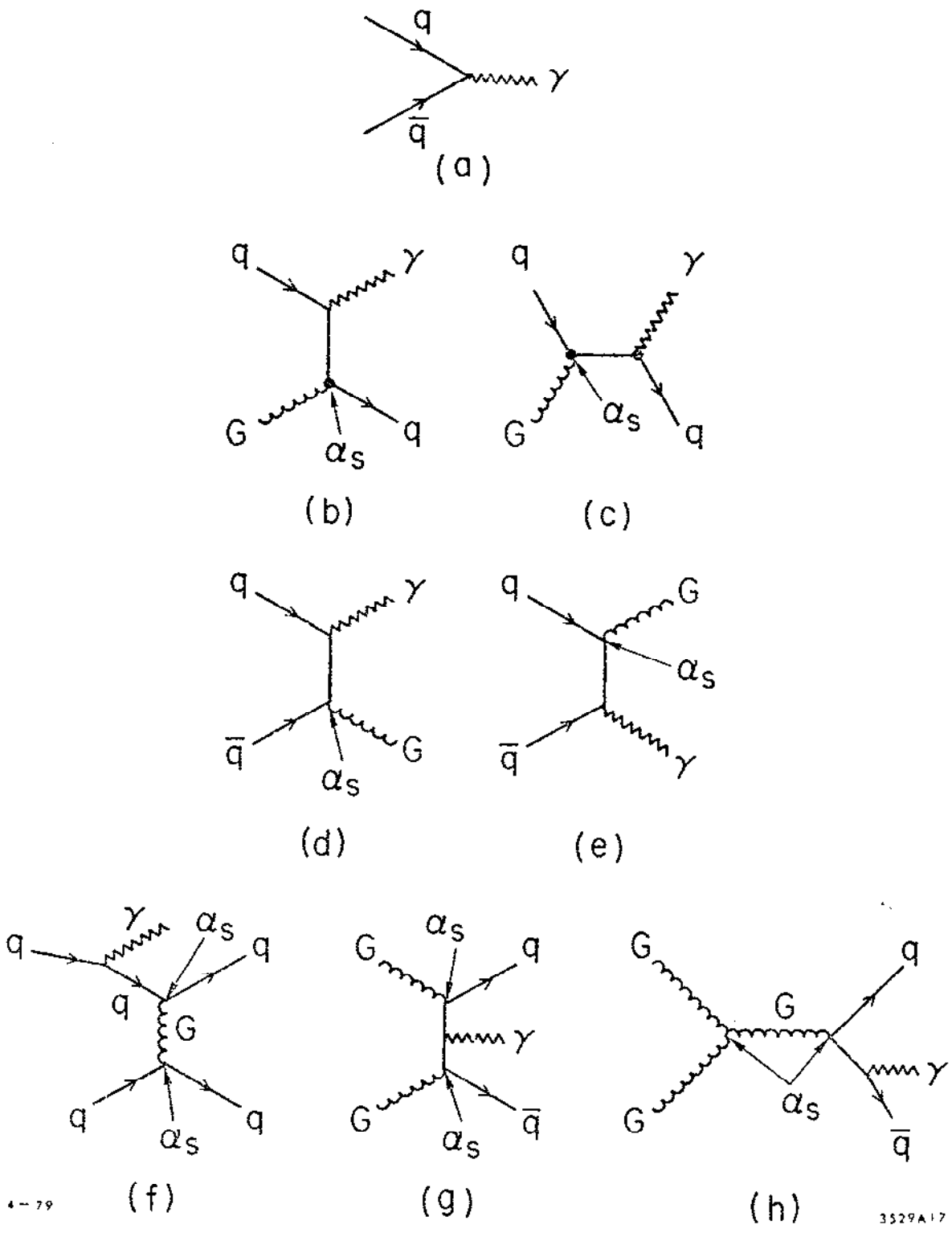
q
γ
q̄
(a)
q
γ
G
αs
q
(b)
q
γ
G
αs
q
(c)
q
γ
q̄
αs
G
(d)
q
G
αs
q̄
γ
(e)
γ
αs
q
q
G
q
q
αs
q
(f)
αs
G
q
γ
G
αs
q̄
(g)
G
q
G
γ
G
αs
q̄
(h)
4-79
3529A17

Fig. 3

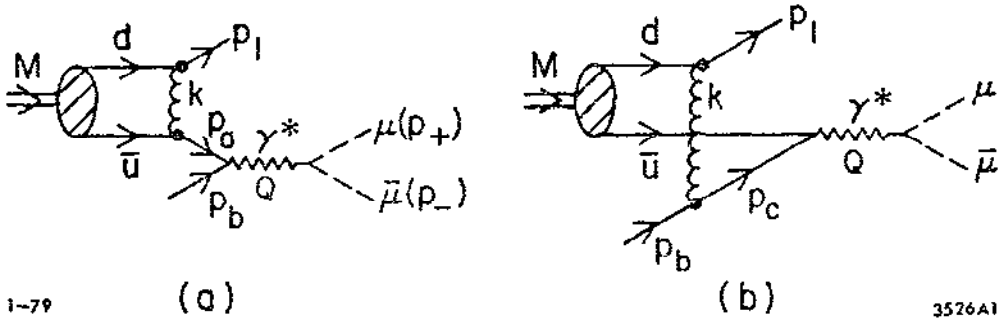
M
d
p_1
k
p_a
γ^*
$\mu(p_+)$
$\bar{u}$
p_b
Q
$\bar{\mu}(p_-)$
1-79
(a)
M
d
p_1
k
γ^*
μ
$\bar{u}$
Q
$\bar{\mu}$
p_c
p_b
(b)
3526A1

Fig. 4

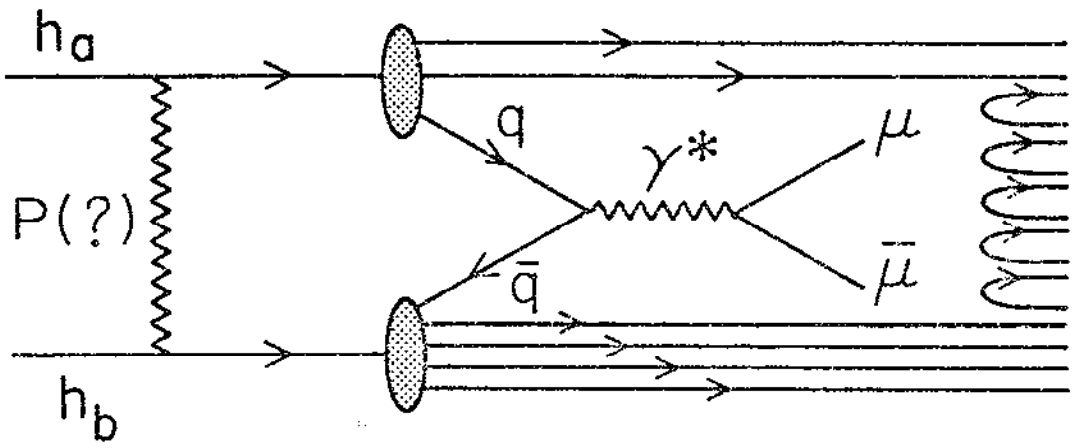

Fig. 5

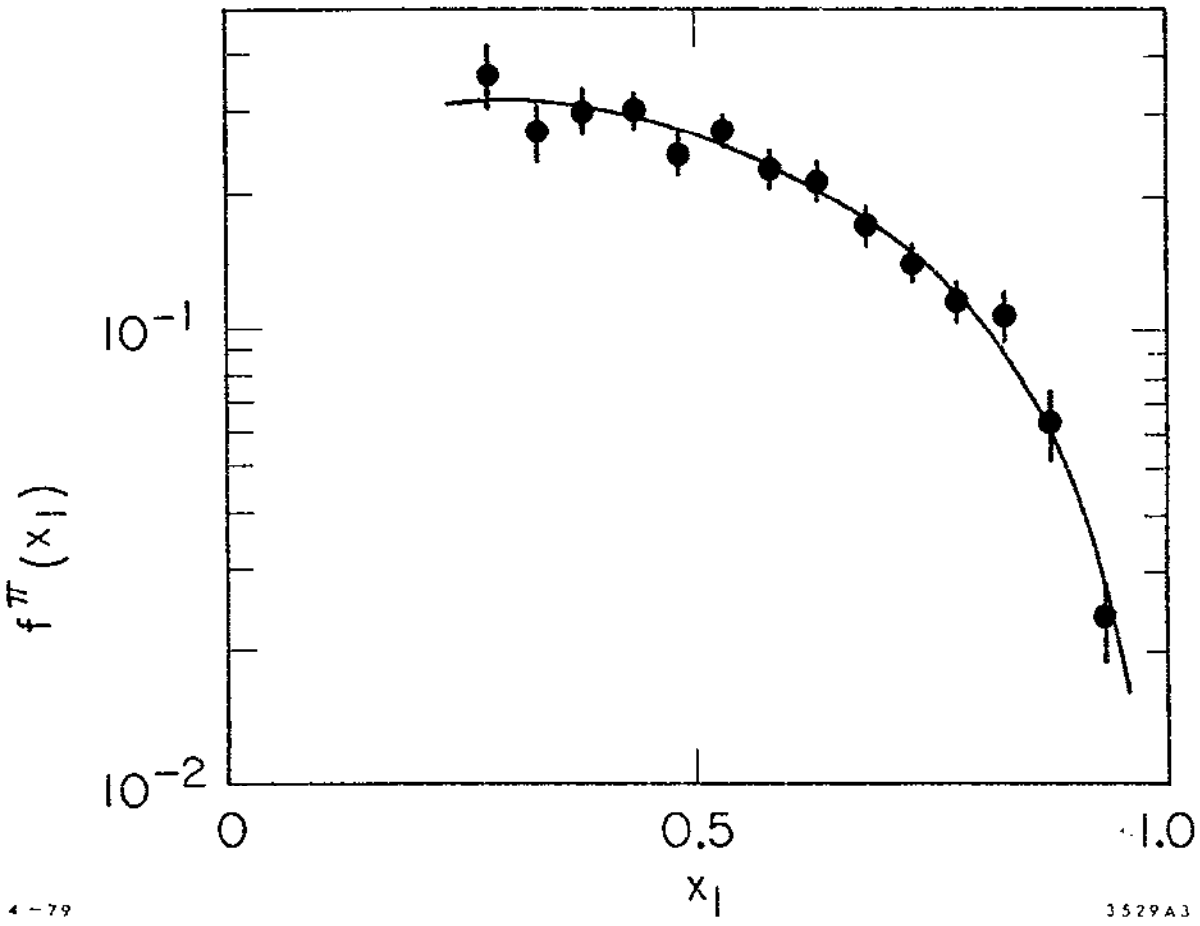

Fig. 6

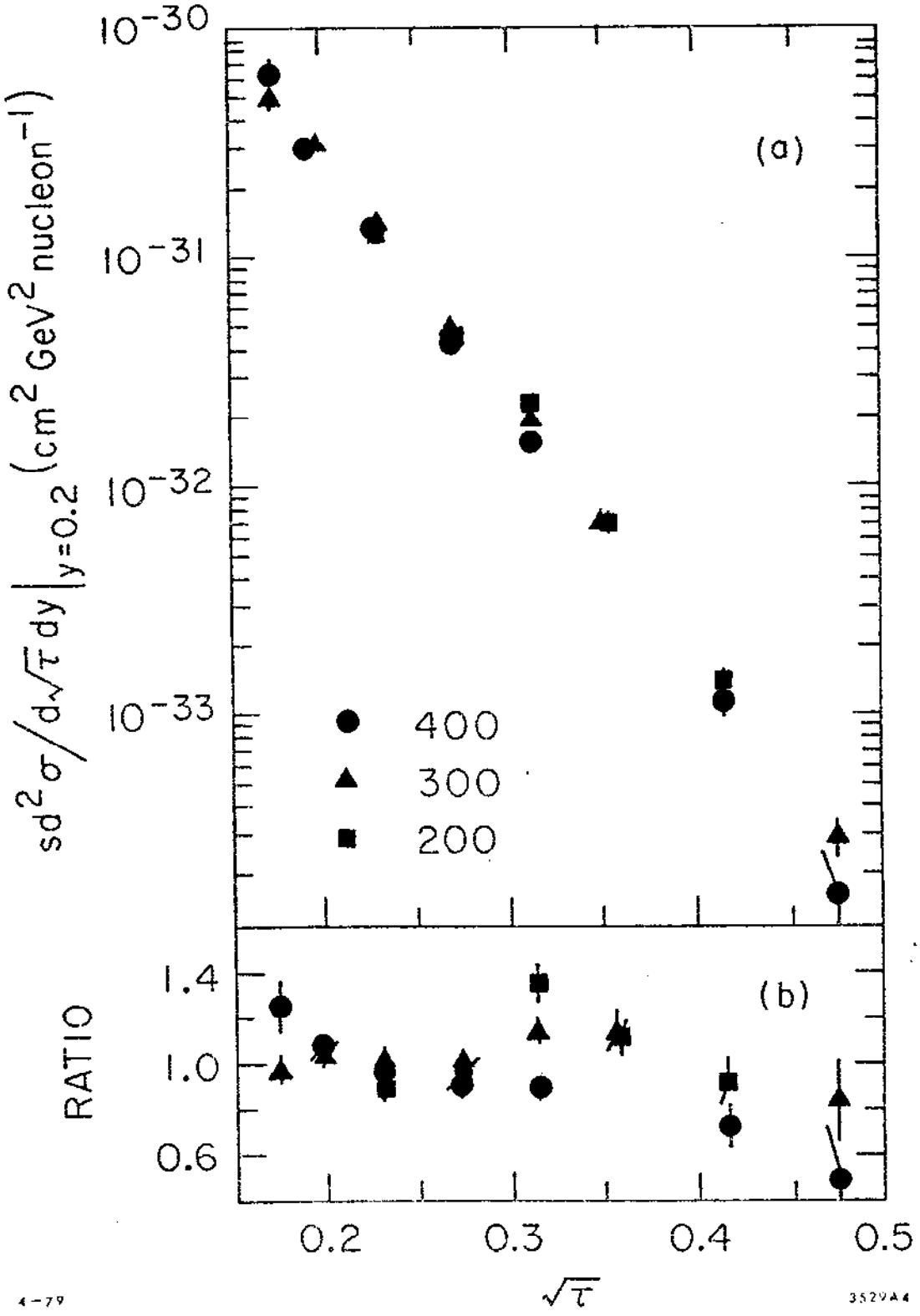
10^{-30}
10^{-31}
10^{-32}
10^{-33}
$sd^2\sigma/d\sqrt{\tau}\,dy\big|_{y=0.2}$ (cm^2 GeV^2 nucleon^{-1})
(a)
400
300
200
RATIO
1.4
1.0
0.6
(b)
0.2
0.3
0.4
0.5
$\sqrt{\tau}$
4-79
3529A4

Fig. 7

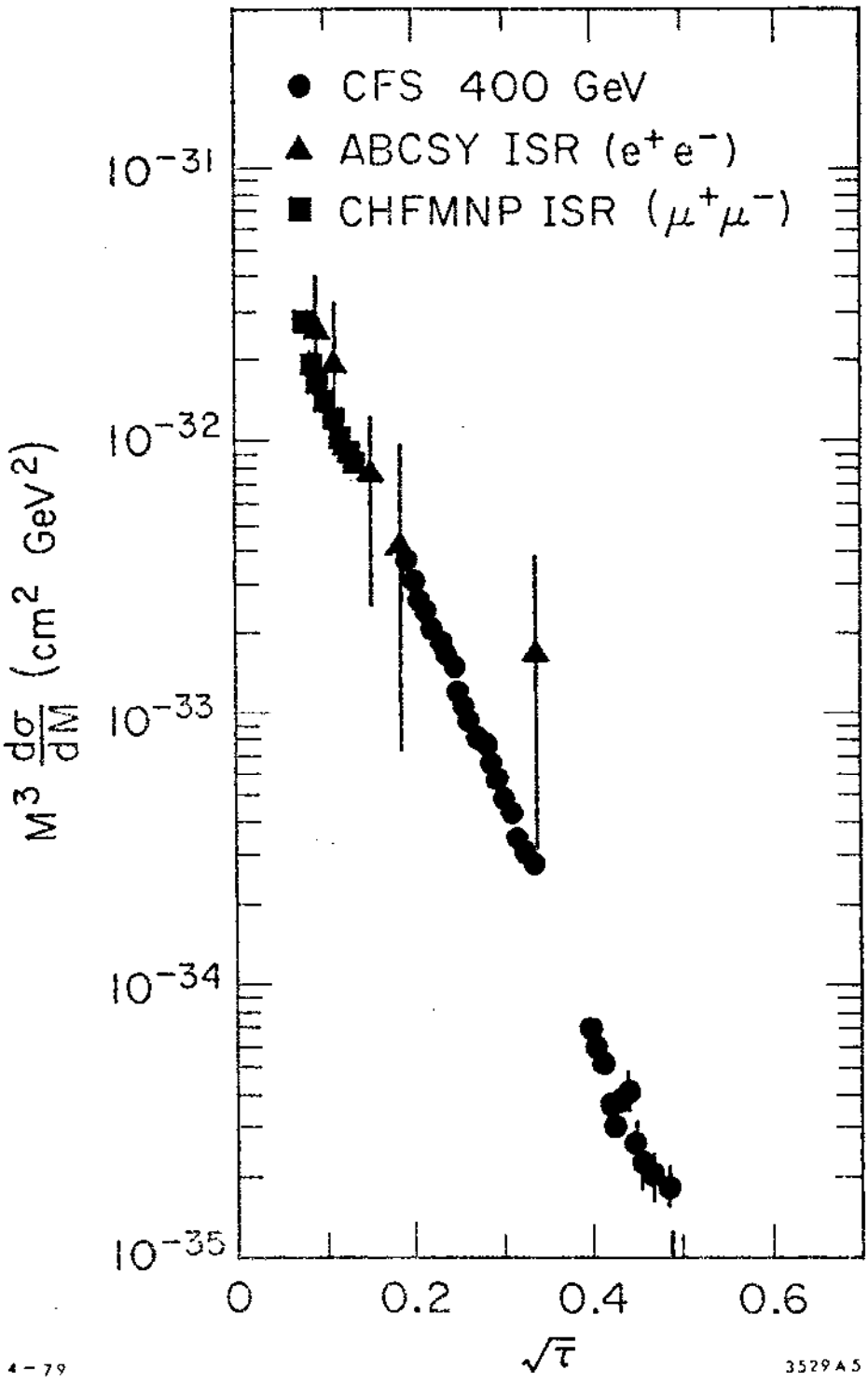
CFS 400 GeV
ABCSY ISR (e+e−)
CHFMNP ISR (μ+μ−)
10−31
10−32
10−33
10−34
10−35
M3 dσ/dM (cm2 GeV2)
0
0.2
0.4
0.6
√τ
4-79
3529A5

Fig. 8

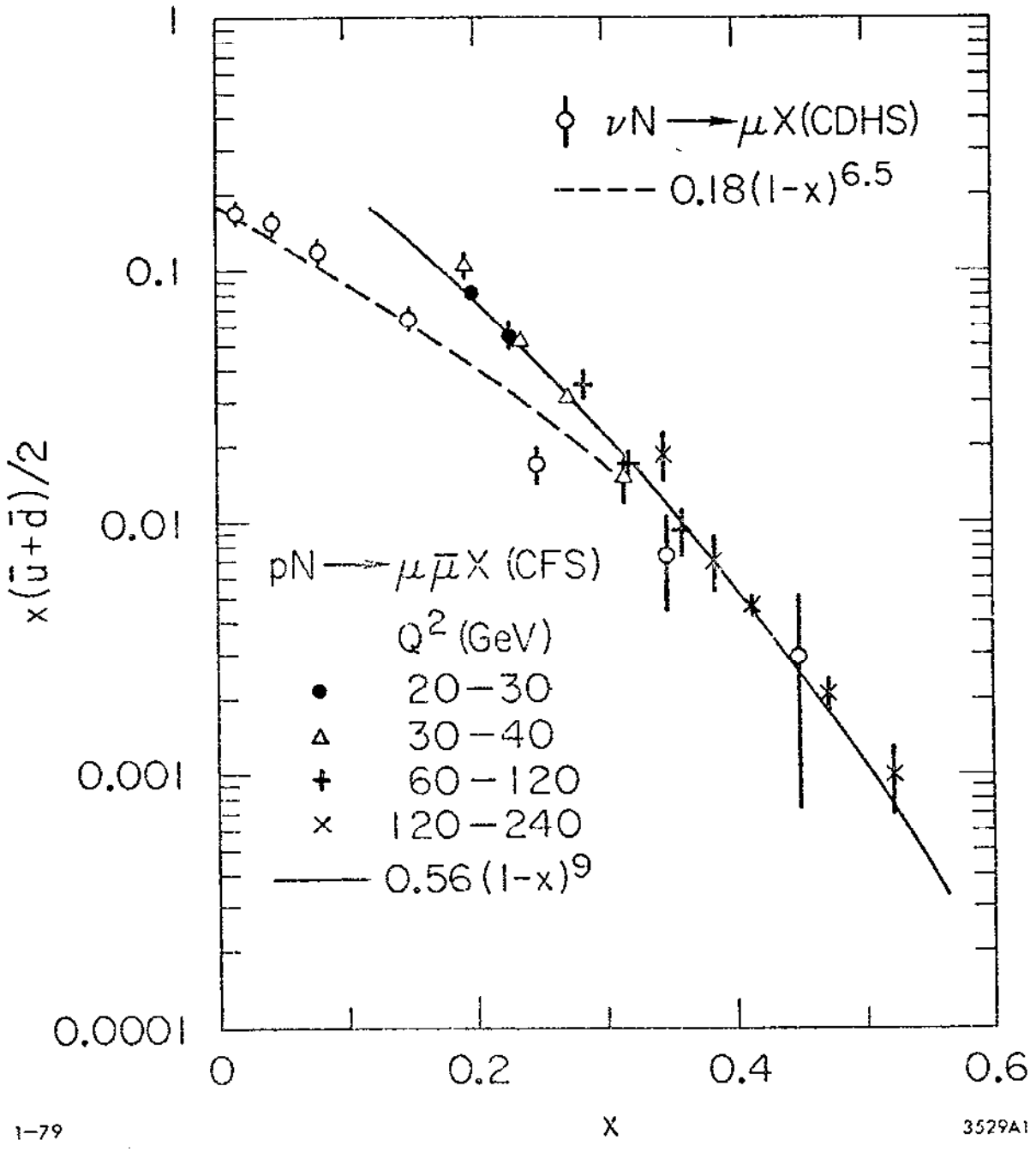
1
0.1
0.01
0.001
0.0001
0
0.2
0.4
0.6
x
$x(\bar{u}+\bar{d})/2$
$\nu N \rightarrow \mu X$(CDHS)
$0.18(1-x)^{6.5}$
$pN \rightarrow \mu\bar{\mu}X$ (CFS)
Q^2 (GeV)
20−30
30−40
60−120
120−240
$0.56(1-x)^9$
1−79
3529A1

Fig. 9

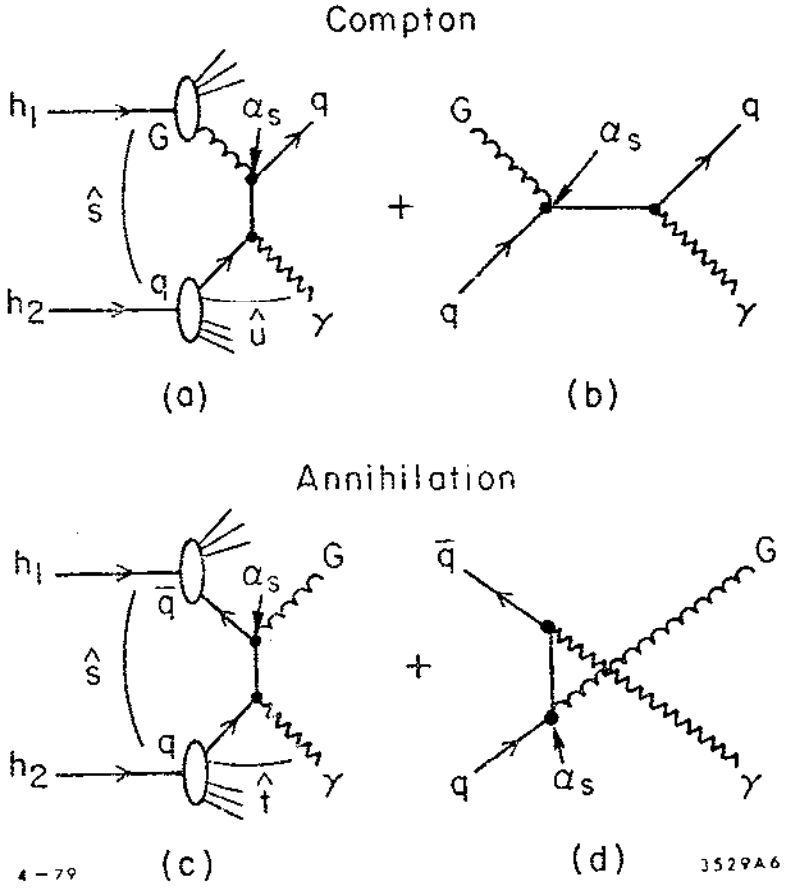
Compton
h_1
G
α_s
q
$\hat{s}$
h_2
q
$\hat{u}$
γ
(a)
+
G
α_s
q
q
γ
(b)
Annihilation
h_1
$\bar{q}$
α_s
G
$\hat{s}$
h_2
q
$\hat{t}$
γ
(c)
+
$\bar{q}$
G
q
α_s
γ
(d)
4-79
3529A6

Fig. 10

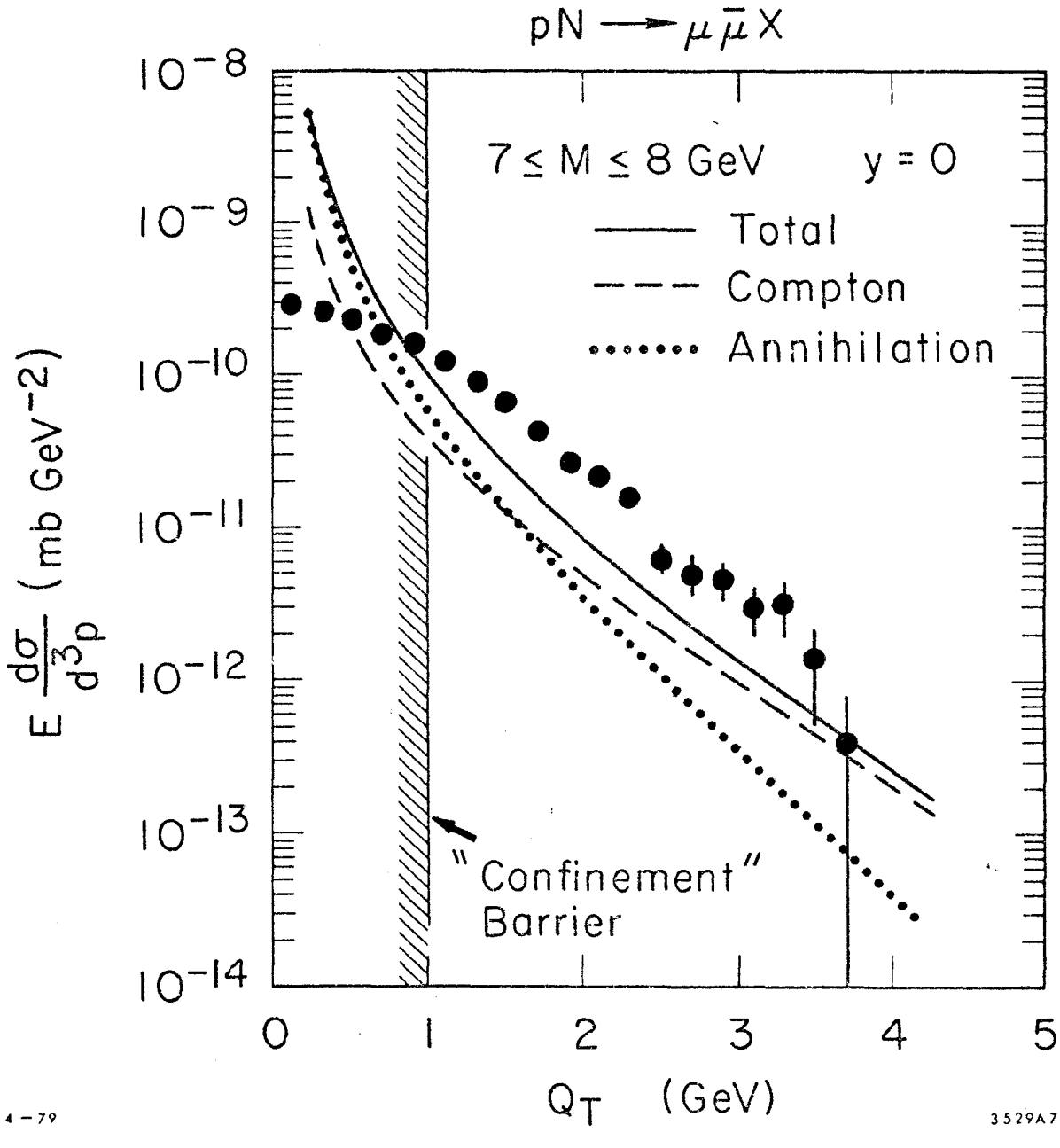
pN → μμ̄X
7 ≤ M ≤ 8 GeV
y = 0
Total
Compton
Annihilation
"Confinement" Barrier
$E\frac{d\sigma}{d^3p}$ (mb GeV^{-2})
10^{-8}
10^{-9}
10^{-10}
10^{-11}
10^{-12}
10^{-13}
10^{-14}
0
1
2
3
4
5
Q_T (GeV)
4-79
3529A7

Fig. 11

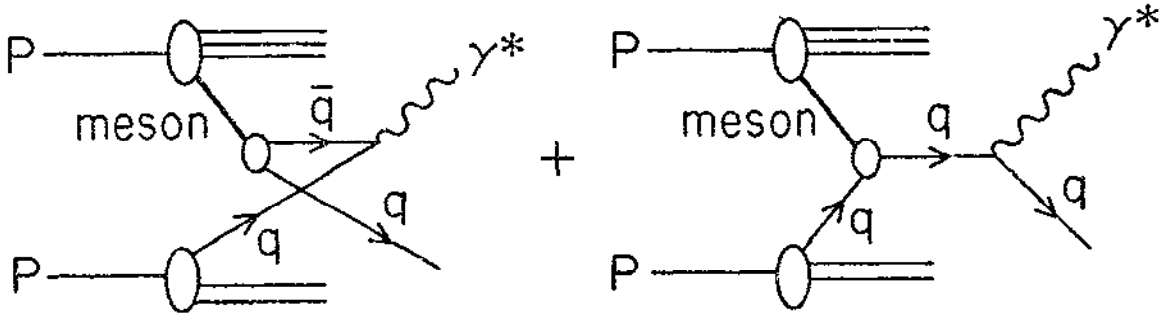

(a)

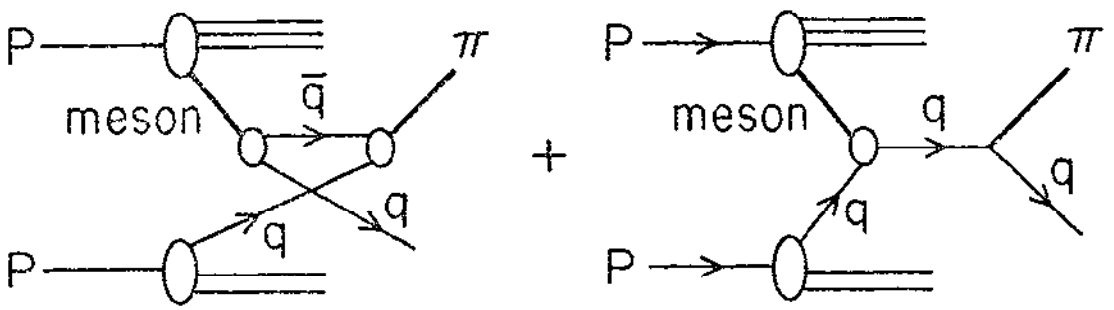

(b)

3 – 78

3370A11

Fig. 12

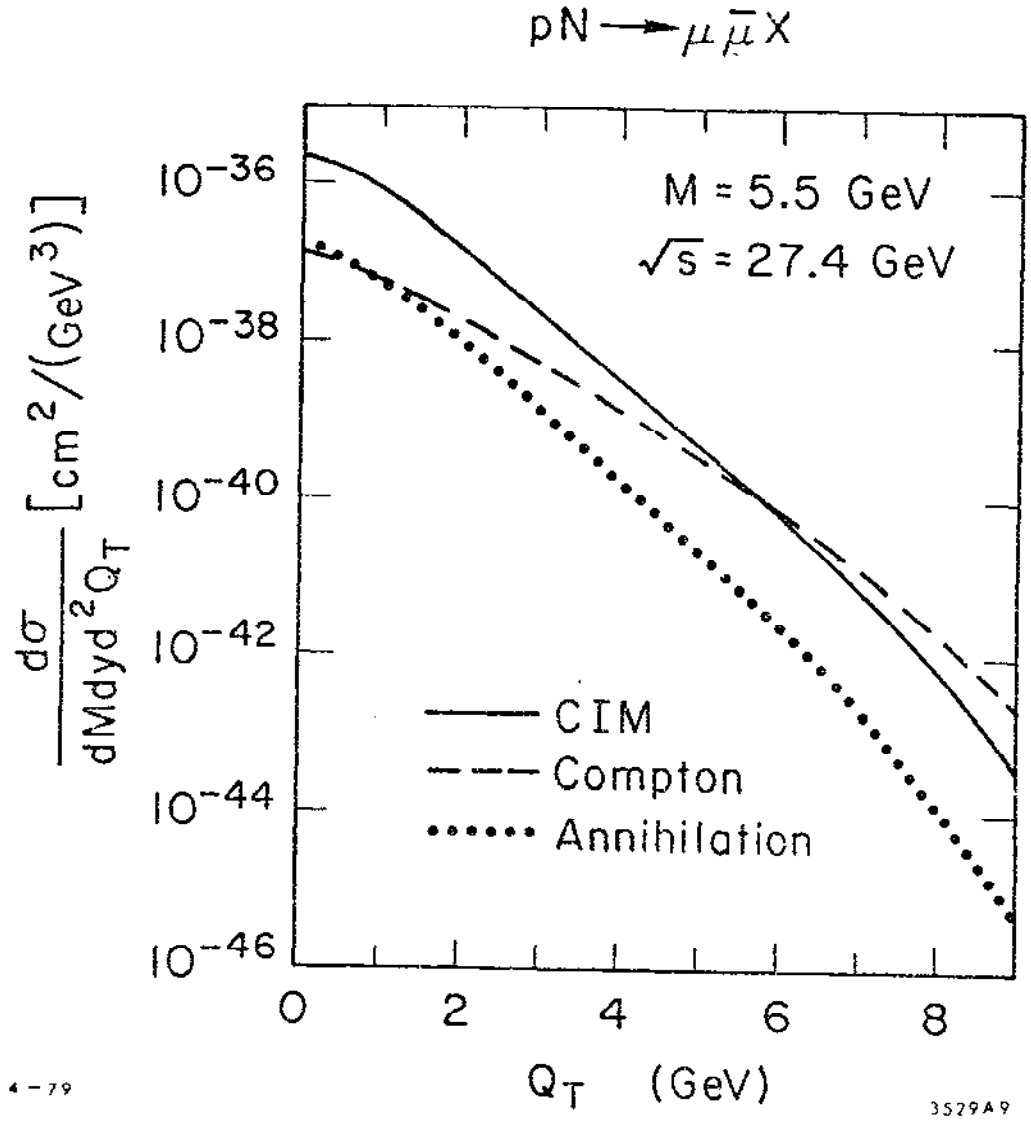
pN → μμ̄X
M = 5.5 GeV
√s = 27.4 GeV
CIM
Compton
Annihilation
10^-36
10^-38
10^-40
10^-42
10^-44
10^-46
0
2
4
6
8
Q_T (GeV)
dσ/dMdyd²Q_T [cm²/(GeV³)]
4-79
3529A9

Fig. 13

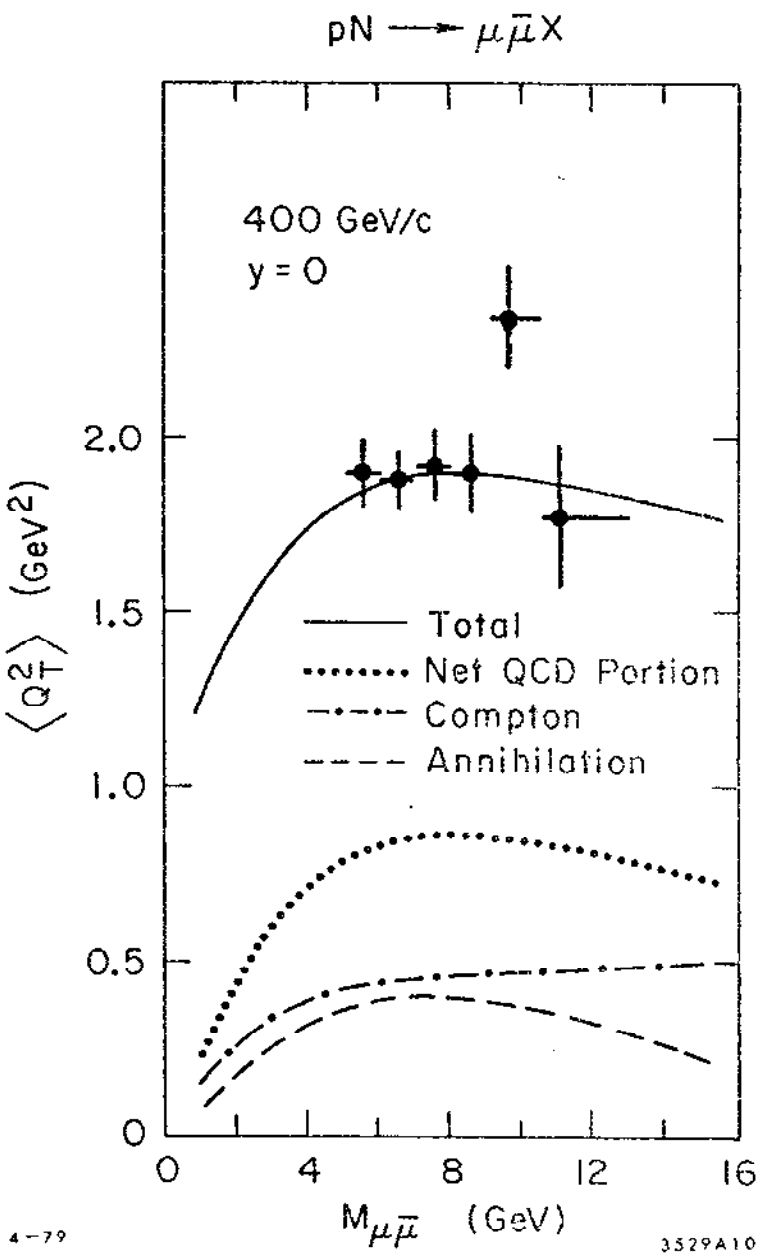
pN → μμ̄X
400 GeV/c
y = 0
2.0
1.5
1.0
0.5
0
⟨Q²T⟩ (GeV²)
Total
Net QCD Portion
Compton
Annihilation
0
4
8
12
16
Mμμ̄ (GeV)
4-79
3529A10

Fig. 14

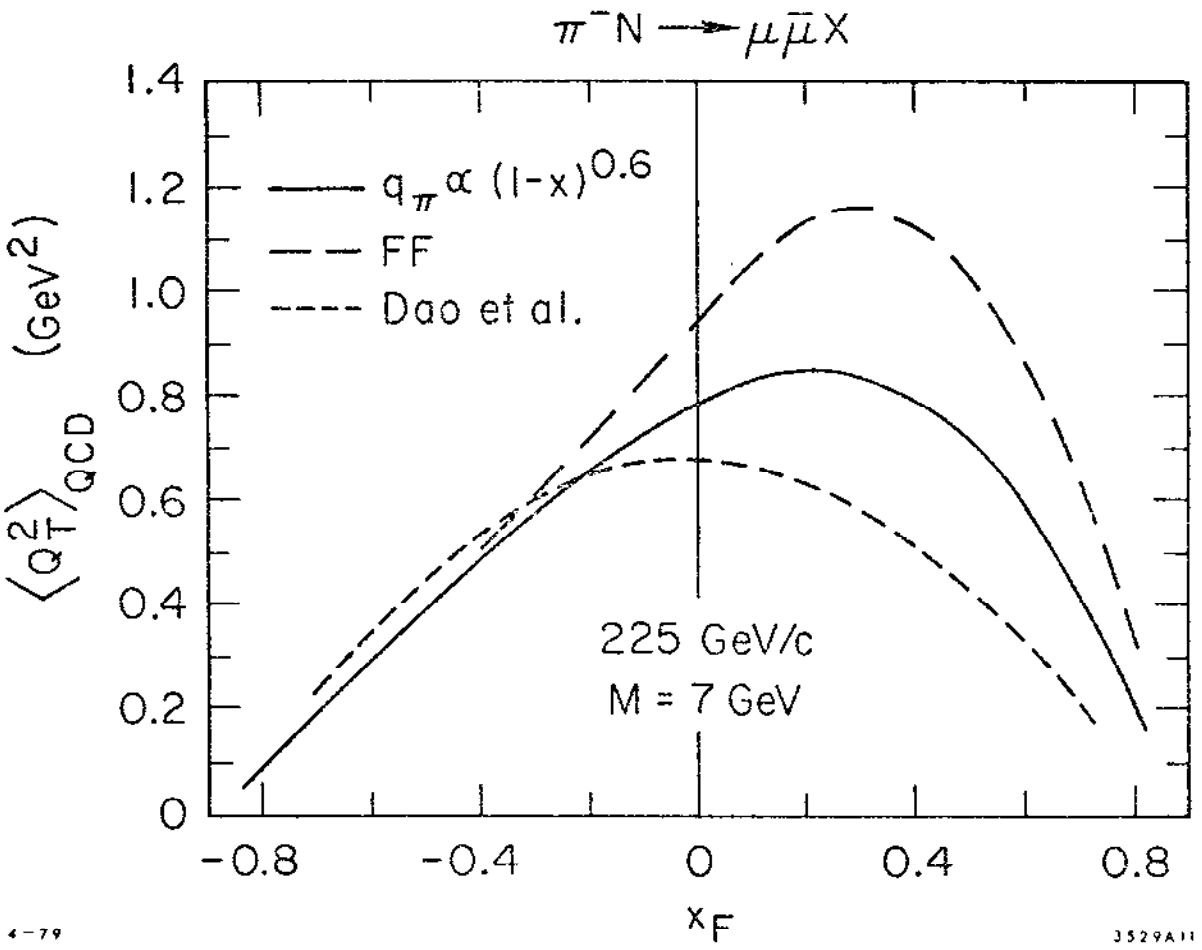
$\pi^- N \rightarrow \mu\bar{\mu} X$
$\langle Q_T^2 \rangle_{QCD}$ (GeV^2)
$q_\pi \alpha (1-x)^{0.6}$
FF
Dao et al.
225 GeV/c
M = 7 GeV
1.4
1.2
1.0
0.8
0.6
0.4
0.2
0
-0.8
-0.4
0
0.4
0.8
x_F
4-79
3529A11

Fig. 15

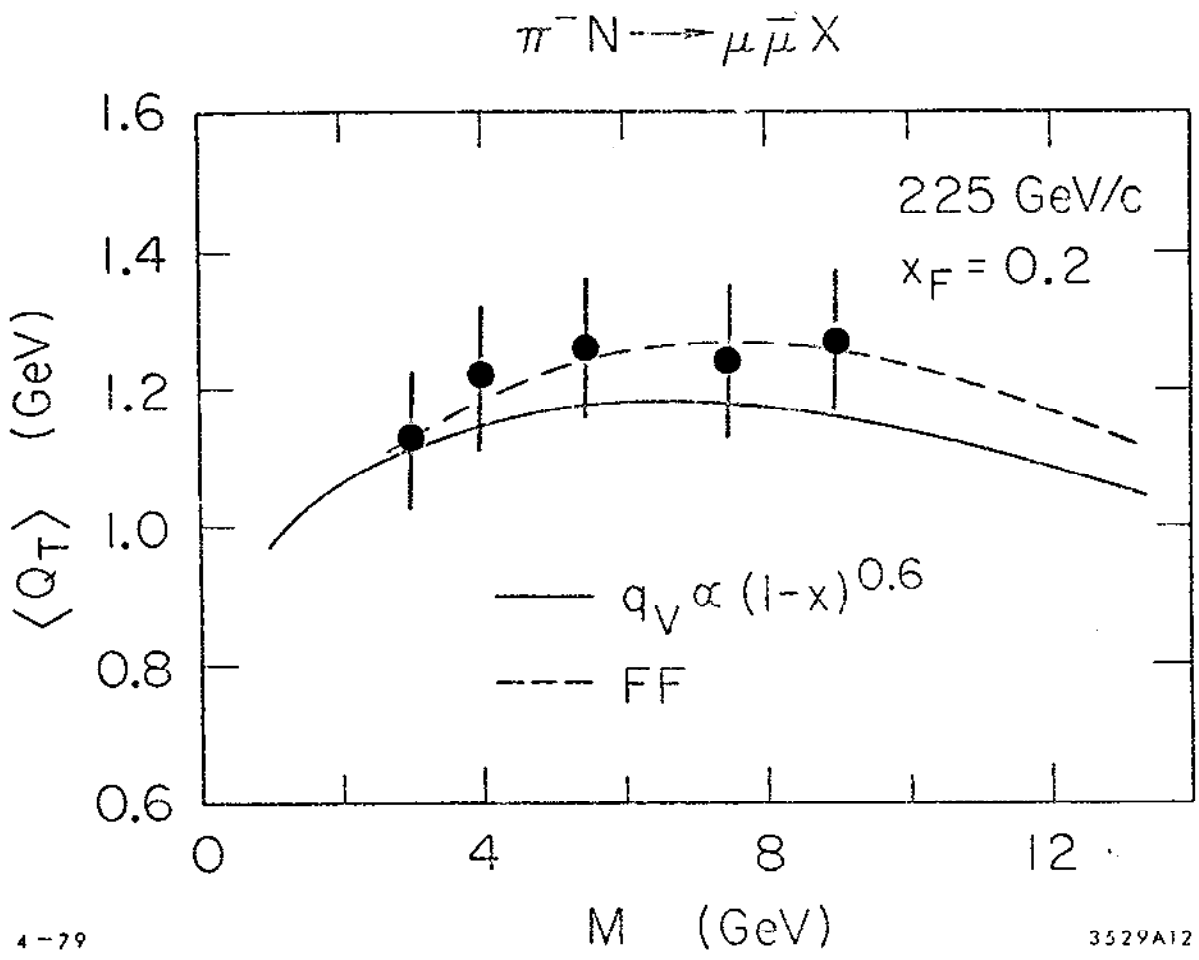
$\pi^- N \longrightarrow \mu\bar{\mu} X$
225 GeV/c
$x_F = 0.2$
$q_V \propto (1-x)^{0.6}$
FF
$\langle Q_T \rangle$ (GeV)
M (GeV)
1.6
1.4
1.2
1.0
0.8
0.6
0
4
8
12
4-79
3529A12

Fig. 16

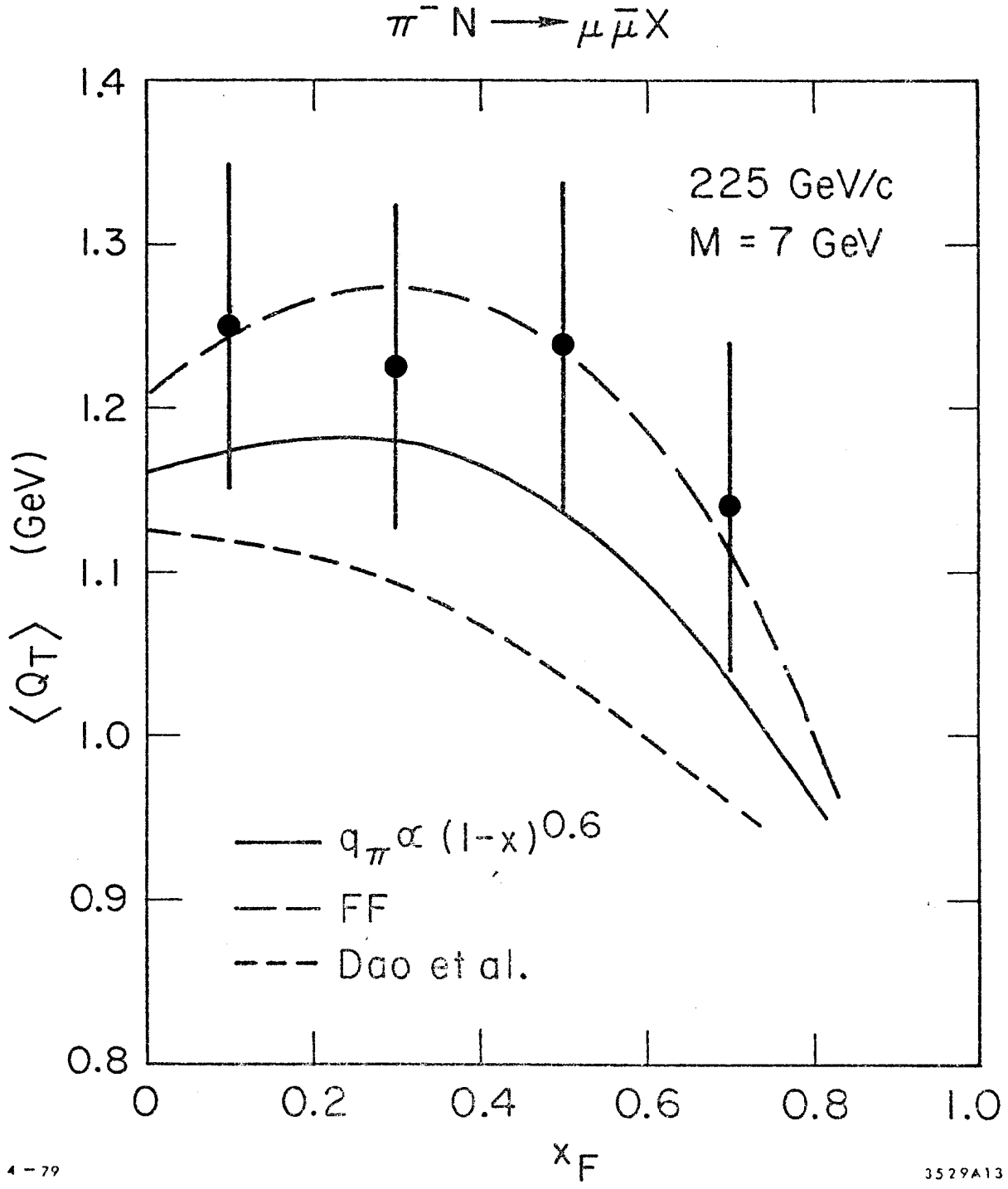
$\pi^- N \longrightarrow \mu\bar{\mu}X$
225 GeV/c
M = 7 GeV
$\langle Q_T \rangle$ (GeV)
1.4
1.3
1.2
1.1
1.0
0.9
0.8
0
0.2
0.4
0.6
0.8
1.0
x_F
$q_\pi \propto (1-x)^{0.6}$
FF
Dao et al.
4 – 79
3529A13

Fig. 17

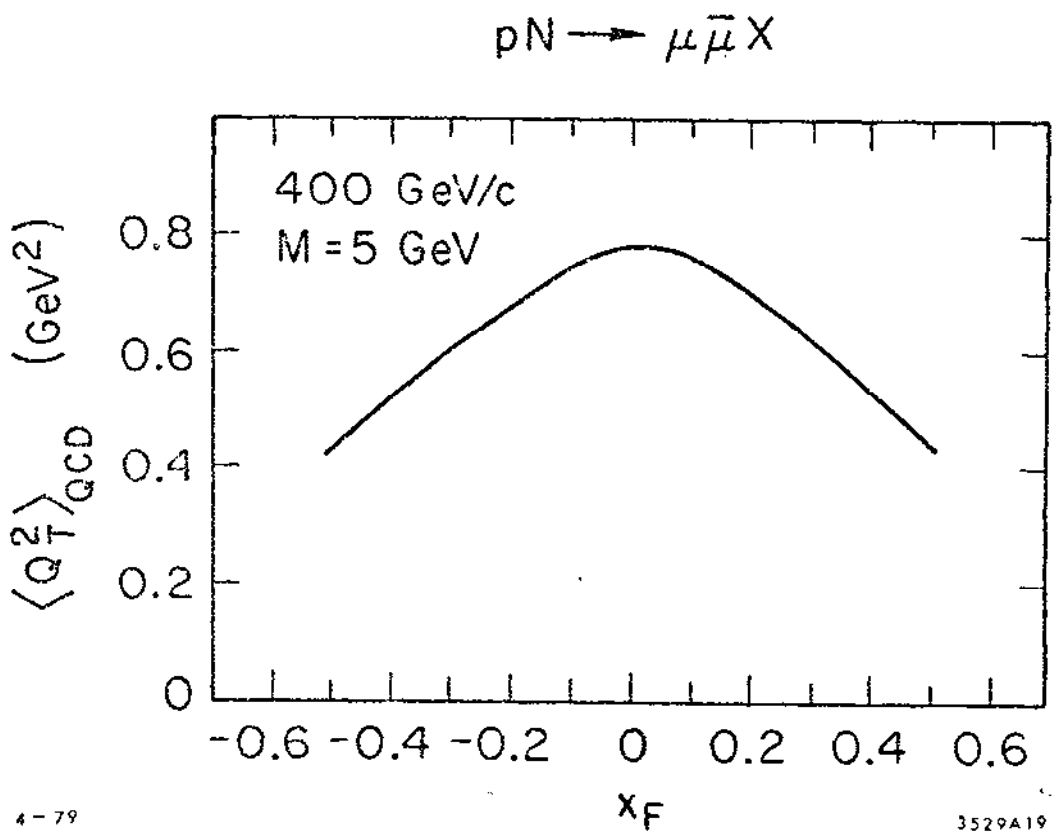
pN → μμ̄X
400 GeV/c
M = 5 GeV
⟨Q_T^2⟩_QCD (GeV^2)
0.8
0.6
0.4
0.2
0
-0.6 -0.4 -0.2 0 0.2 0.4 0.6
x_F
4-79
3529A19

Fig. 18

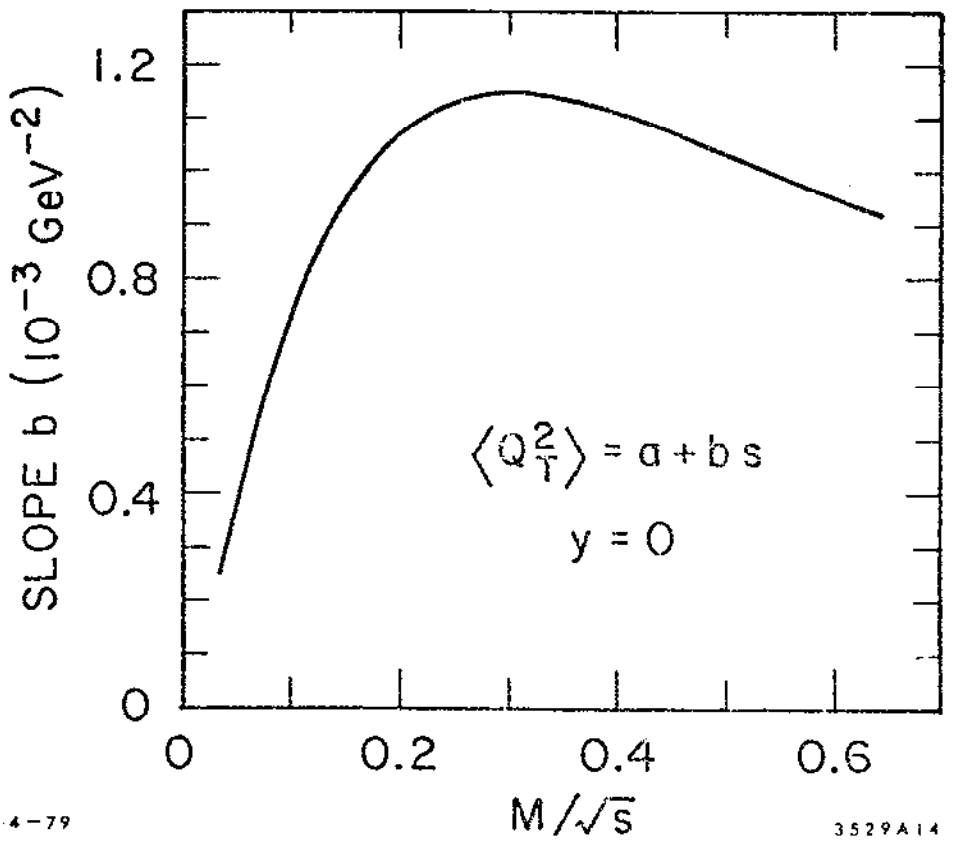
SLOPE b (10^{-3} GeV^{-2})
1.2
0.8
0.4
0
0
0.2
0.4
0.6
$M/\sqrt{s}$
$\langle Q_T^2 \rangle = a + b\,s$
$y = 0$
4-79
3529A14

Fig. 19

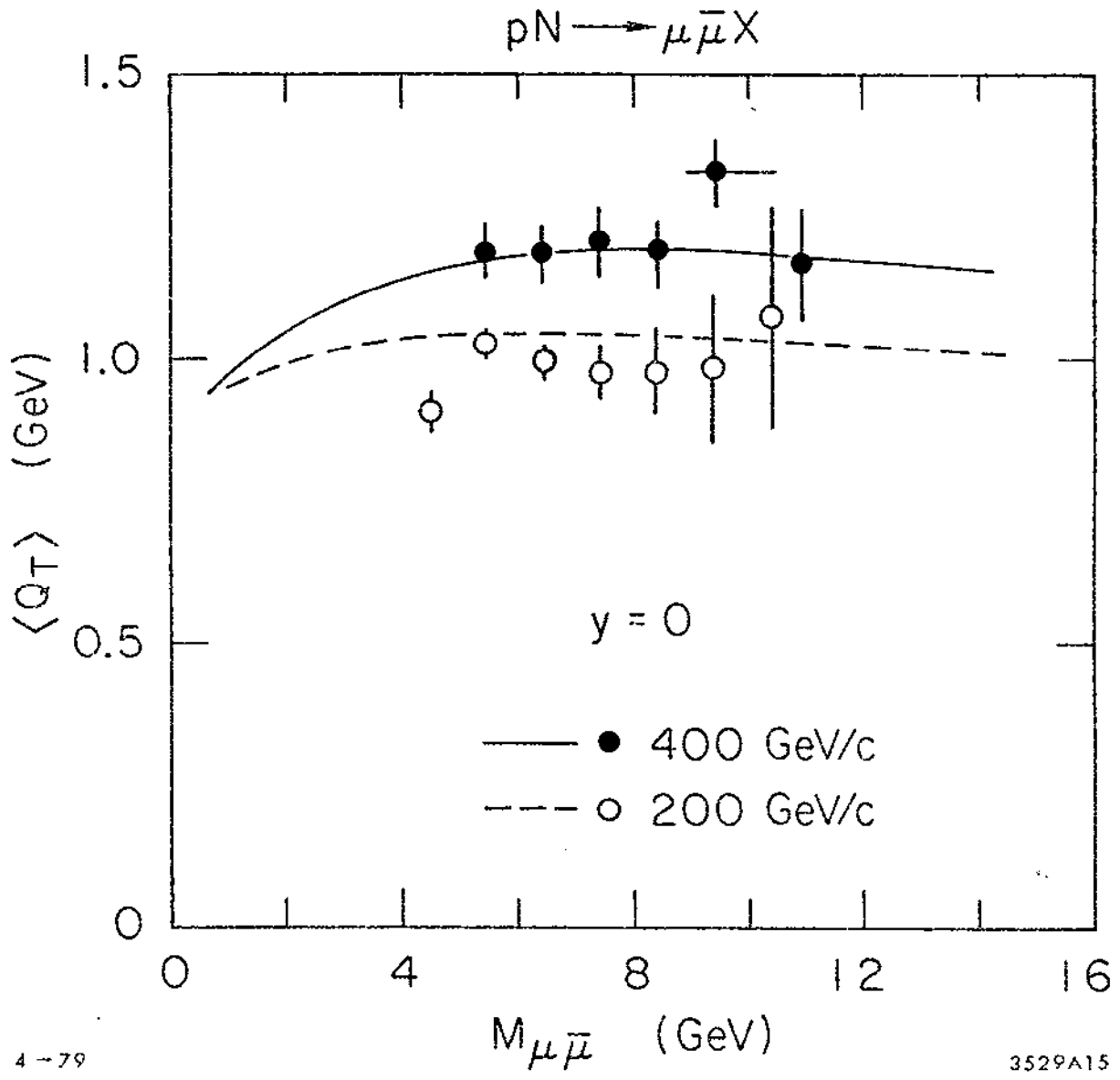
pN → μμ̄X
1.5
1.0
0.5
0
⟨Q_T⟩ (GeV)
y = 0
400 GeV/c
200 GeV/c
0
4
8
12
16
M_μμ̄ (GeV)
4-79
3529A15

Fig. 20